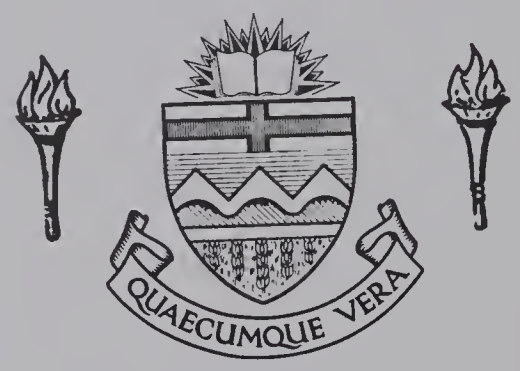

THE UNIVERSITY OF ALBERTA

BLOOD FLOW IN A LARGE ARTERIAL BIFURCATION

BY

© DARREL H. HOWELL

A THESIS

SUBMITTED TO THE FACULTY OF GRADUATE STUDIES

IN PARTIAL FULFILMENT OF THE REQUIREMENTS FOR THE DEGREE

OF MASTER OF SCIENCE

DEPARTMENT OF MECHANICAL ENGINEERING

EDMONTON, ALBERTA

FALL, 1970

UNIVERSITY OF ALBERTA

FACULTY OF GRADUATE STUDIES

The undersigned certify that they have read, and recommend to the Faculty of Graduate Studies for acceptance, a thesis entitled "BLOOD FLOW IN A LARGE ARTERIAL BIFURCATION" submitted by Darrel H. Howell in partial fulfilment of the requirements for the degree of Master of Science.

ABSTRACT

An experimental investigation is presented for the problem of the effect of varying the significant dimensionless parameters on the manner in which the flow divides at an arterial bifurcation.

An experimental apparatus was designed and constructed to simulate the physiological range of these parameters. The only type of bifurcation examined was the "side branch", where a single branch of smaller dimensions leaves the parent trunk at an angle dependent on the anatomical position.

The mass flow ratio (the ratio of the flow rate in the small branch to the flow rate in the large branch) was found to be directly proportional to the unsteadiness parameter, the normalized velocity fluctuation, and the branch diameter ratio, and inversely proportional to the Reynolds number.

Some observations of the physical flow characteristics were made using a photographic technique.

ACKNOWLEDGEMENTS

The author wishes to thank the following for their contributions:

- Dr. C.M. Rodkiewicz for supervising the thesis.
- Dr. N.R. Kuchar of the General Electric Space Sciences Laboratory in Philadelphia who suggested the problem to Dr. Rodkiewicz during their meeting at the University of Michigan in the summer of 1968. Dr. Kuchar's guidance during the course of the thesis work was also appreciated.
- Dr. R.D. Laurenson of the Department of Anatomy, University of Alberta for his helpful suggestions.
- Mr. Phung Quoc Hoc, B.Sc. (Alberta, 1970), for his assistance in the construction of the experimental apparatus during the summer of 1969.
- Mr. Ted Gates and Mr. Bob Romanko for their assistance in conducting the experiments during the summer of 1970.
- Miss Helen Wozniuk for typing the thesis.
- My wife, Liz, for her patience.

TABLE OF CONTENTS

		Page
Title Page		i
Approval Sheet		ii
Abstract		iii
Acknowledgements		iv
Table of Contents		v
List of Tables		vii
List of Figures		ix
List of Symbols		xi
CHAPTER I	INTRODUCTION	
	1.1 Introductory Remarks	1
	1.2 Blood and the Circulatory System	2
	1.3 Literature Survey	7
	1.4 Objectives of the Thesis	9
CHAPTER II	THE MATHEMATICAL MODEL	
	2.1 Introductory Remarks	10
	2.2 Simplifications Employed in the Mathematical Model	10
	2.3 Derivation of the Parameters	12
CHAPTER III	THE EXPERIMENTAL MODEL	
	3.1 The Range of Study	20

TABLE OF CONTENTS (continued)

		Page
CHAPTER III	(continued)	
	3.2 Design of the Model	24
	3.3 Description of the Apparatus	26
	3.3.1 The Test Section	26
	3.3.2 The Flow Unit	31
	3.3.3 Miscellaneous	32
CHAPTER IV	THE EXPERIMENTS	
	4.1 Summary of Parameters and Ranges of Study .	35
	4.2 The Mass Flow Ratio	35
	4.2.1 The Mass Flow Ratio as a Function of the Unsteadiness Parameter and the Normalized Fluctuating Component of Velocity	37
	4.2.2 The Mass Flow Ratio as a Function of the Unsteadiness Parameter and the Reynolds Number	42
	4.2.3 The Mass Flow Ratio as a Function of the Bifurcation Geometry	42
	4.3 Description of the Flow	42
CHAPTER V	CONCLUDING REMARKS	
	5.1 Observations and Discussion	56
	5.2 Summary	58
	5.3 Suggestions for Further Work	58

TABLE OF CONTENTS (continued)

		Page
REFERENCES		62
APPENDIX A	SPECIFIC GRAVITY AND VISCOSITY OF THE BLOOD ANALOGUE	64
APPENDIX B	PISTON STROKE CALCULATIONS	70
APPENDIX C	CAM DESIGN	74
APPENDIX D	MANOMETER CALIBRATION CURVES	76
APPENDIX E	SUGGESTIONS FROM THE ORAL EXAMINATION (DEFENSE OF THESIS)	78
	E.1 The Length Ratio	78
	E.2 Units of Pulse Rate	78
	E.3 Dr. Laurenson's Suggestions	79

LIST OF TABLES

Table		Page
4.1	The Dimensionless Parameters and their Ranges of Study	36
4.2	Dependence of γ on a for λ = 1.0, Re = 1630, β = 0.60, θ = 50°	38
4.3	Dependence of γ on a for λ = 1.5, Re = 1630, β = 0.60, θ = 50°	39
4.4	Dependence of γ on a for λ = 2.0, Re = 1630, β = 0.60, θ = 50°	40
4.5	Dependence of γ on a for λ = 2.0, Re = 1330, β = 0.60, θ = 50°	43
4.6	Dependence of γ on a for λ = 2.0, Re = 2000, β = 0.60, θ = 50°	44
4.7	Mass Flow Ratio as a Function of Bifurcation Geometry..	46
A.1	The Viscosities of Various Glycerin/Water Mixtures	65

LIST OF FIGURES

Figure		Page
1.1	Schematic of the Circulatory System	3
1.2	Photograph of Silicone Polymer Cast of Cat's Aorta and its Major Branches	4
1.3	Cross-Section of a Coronary Artery with Severe Atherosclerotic Plaque Formation	4
2.1	The Coordinate System	13
3.1	Experimental Simulation of Flow From the Heart	22
3.2	The Experimental Bifurcation	23
3.3	Schematic of the Apparatus	
3.4	Photograph of the Experimental Model	28
3.5	Typical Glass Bifurcations	30
3.6	Photograph of the Test Section	30
3.7	Photographs of the Flow Unit	33
4.1	Mass Flow Ratio γ vs Unsteadiness Parameter a for $\lambda = 1.0, 1.5, 2.0$, $\beta = \frac{0.75}{1.25} = 0.60$; $\theta = 50°$; Re = 1630	41
4.2	Mass Flow Ratio γ as a Function of Unsteadiness Parameter a and Reynolds Number Re $\beta = \frac{0.75}{1.25} = 0.60$ $\theta = 50°$ $\lambda = 2.0$	45
4.3	Mass Flow Ratio γ vs Diameter Ratio β as a Function of Re $\theta = 50°$, a = 10.2, $\lambda = 2.0$	47

LIST OF FIGURES (continued)

Figure		Page
4.4	Mass Flow Ratio γ vs Diameter Ratio β as a Function of λ $\theta = 50°$, $a = 6.50$, $Re = 1630$	48
4.5	Mass Flow Ratio γ vs Diameter Ratio β as a Function of a $\theta = 50°$, $\lambda = 2.0$, $Re = 1630$	49
4.6	Mass Flow Ratio γ vs Angle of Branching θ as a Function of a and λ $Re = 1630$, $\beta = 0.60$	50
4.7	Mass Flow Ratio γ vs Angle of Branching θ as a Function of Re $a = 10.2$, $\lambda = 2.0$, $\beta = 0.60$	51
4.8	Physical Description of the Flow	52
4.9	Flow Characteristics for Various Angles of Branching $\beta = 0.80$ $Re = 1850$	54
4.10	Flow Characteristics for Various Reynolds Numbers $\beta = 0.60$ $\theta = 50°$	55
A.1	Viscosity vs Temperature of 39.31% (by weight) Glycerin/Water Mixture	66
A.2	Viscosity vs Temperature of 99.14% (by weight) Glycerin/Water Mixture	67
A.3	Viscosity vs Weight Percent Glycerin at 20°C	68
B.1	Flow in the Experimental Model	71
C.1	Cam Design	75
D.1	Manometer Calibration Curves	77

LIST OF SYMBOLS

a	unsteadiness parameter ($D \sqrt{\frac{\omega}{\nu}}$)
d	unstressed internal diameter of side branch
D	unstressed internal diameter of main branch
$F_x(m)$, $F_r(m)$, $F_\phi(m)$	longitudinal, radial, and azimuthal components of applied body force per unit mass of fluid
ℓ	length of piston stroke
L	approximate length of entrance region
L_e	length ratio (R_o/L)
P	static pressure
ΔP	average pressure drop in entrance region
$\bar{q}$	vectorial fluid velocity
Q	total flow rate ($Q_d + Q_D$)
Q_d	flow rate in side branch
Q_D	flow rate in main branch
r	radial space coordinate
R_o	unstressed internal radius
Re	Reynolds number (UR_o/ν)
Str	Strouhal number (L/UT_o)
t	time variable
T_o	period for one pulse
u	longitudinal coordinate of velocity

U	average longitudinal velocity
U'	fluctuating component of longitudinal velocity
v	radial coordinate of velocity
V	reference radial velocity
w	azimuthal coordinate of velocity
x	longitudinal space coordinate
β	ratio of branch diameters (d/D)
γ	mass flow ratio (Q_d/Q_D)
θ	angle of branching
λ	normalized velocity fluctuation (U'/U)
μ	absolute fluid viscosity
ν	kinematic fluid viscosity (μ/ρ_f)
ρ_f	fluid density
ϕ	azimuthal space coordinate
ω	pulse rate

CHAPTER I

INTRODUCTION

1.1 Introductory Remarks

Because of the prevalence of diseases and defects of the cardiovascular system, researchers are expending considerable energy studying this complex system. An engineer's background in applicable fields like fluid mechanics would appear to make him a natural for research in this field. A survey of recent literature in the field of cardiovascular research indicates that significant contributions are being made by individuals from engineering and related fields.

The purpose of this thesis is to study certain aspects of blood flow in a large arterial bifurcation. The author has relied heavily on Dr. N.R. Kuchar's Ph.D. thesis [1] and his recent paper on blood flow devices [2] for the necessary theoretical background. Dr. Kuchar's publications to date have been highly mathematical and concerned with blood flow in a straight tube. By contrast this project is entirely experimental and concerned with branching vessels.

Because this thesis is being done in the Department of Mechanical Engineering, it seems quite likely that many people lacking a formal medical or physiological background may read it. It is for this reason that Section 1.2, a resumé of some of the properties and characteristics of the circulatory system, has been included. This section comes before

the literature survey in the hope that any unfamiliar terms used in the survey will have been explained adequately in Section 1.2.

The purpose of the literature survey is threefold. First, the author has attempted to outline the work on flow in straight, unbranching tubes that has led up to this thesis. Second, some of the related work being done on branched tubes has been reviewed. Third, by referring to some of the points made by other authors, an attempt has been made to further justify undertaking this type of research.

1.2 Blood and the Circulatory System

The circulatory system is illustrated schematically in Figure 1.1. Oxygen-rich blood from the lungs enters the left side of the heart and is expelled into the aorta by contraction of the heart. The blood is distributed to the capillary networks of the various organs by the multi-branched arterial system. The complexity of this system is illustrated by Figure 1.2, a photograph of a silicone polymer cast of a cat's aorta and major branches. The blood exchanges oxygen, carbon dioxide, foodstuffs, and metabolites with the tissues across the capillary membrane. The deoxygenated blood is collected by the venous system and returned to the lungs via the vena cava and the right side of the heart.

The heart produces a periodic or pulsatile flow on the arterial or high pressure side of the system. The amplitude of the pulse is largest in the aorta and becomes gradually smaller as the system branches. This decrease is caused by the dampening effect of the highly elastic arterial walls. Further dampening in the capillary system results in

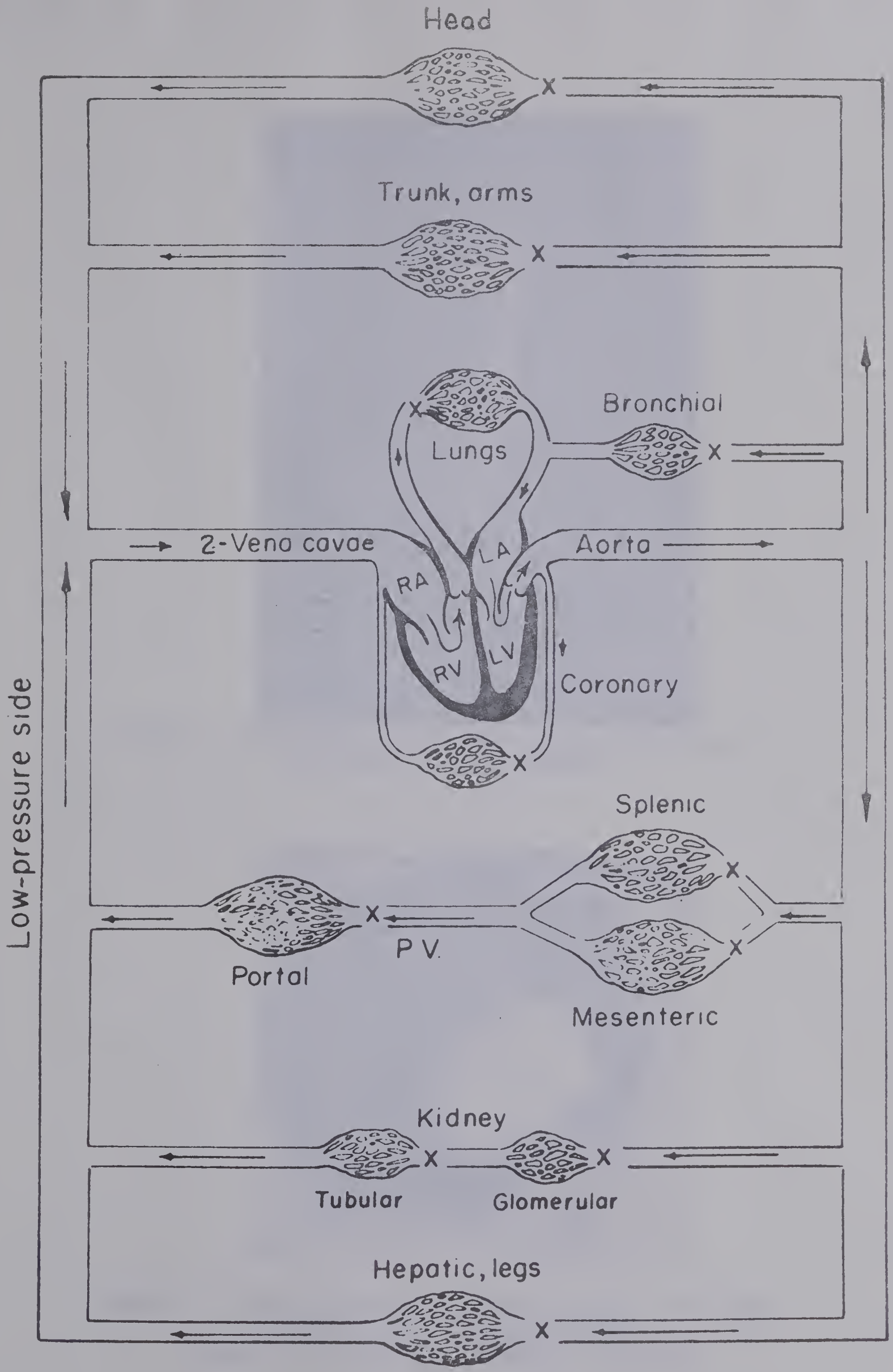

FIGURE 1.1 SCHEMATIC OF THE CIRCULATORY SYSTEM

FIGURE 1.2 PHOTOGRAPH OF SILICONE POLYMER CAST OF CAT'S AORTA AND ITS MAJOR BRANCHES

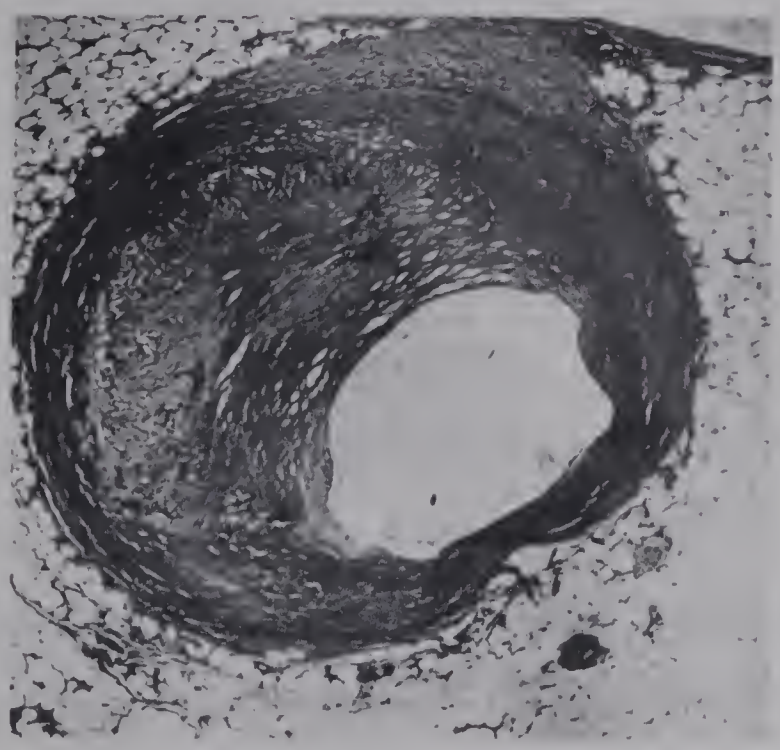

FIGURE 1.3 CROSS-SECTION OF A CORONARY ARTERY WITH SEVERE ATHEROSCLEROTIC PLAQUE FORMATION
(COURTESY OF PROVINCIAL LABORATORY, EDMONTON)

steady flow in the venous system. Because the walls of the venous system are subjected to much less pressure and pressure variation, they are thinner and contain less elastin than the arterial vessels. Elastin is the component of vessel walls largely responsible for their elasticity. Further characteristics of the vessel walls are discussed in detail by McDonald [3] and Whitmore [4].

Despite the extra strength and elasticity of the arterial walls, it seems likely that a system under the continual wear and tear of a pulsatile flow would be subject to many disorders. Such is the case, arterial disease being a very great problem. Mitchell and Schwartz [5] note that authors have classified arterial disorders by such names as arteriosclerosis, atheroma, and atherosclerosis. The most widely adopted term, atherosclerosis, will be used in this thesis. It will refer to the build up of fatty and/or fibrous plaques which occlude the vessel and destroy the elasticity of its walls. Figure 1.3 is a photograph of the cross-section of a coronary artery that has been severely occluded by atherosclerotic plaque formation.

Blood consists of cells called the formed elements suspended in an intracellular fluid called the plasma. The formed elements are the red blood cells, the white blood cells, and the platelets.

The red blood cell is a biconcave discoidal cell of 7 microns length and 2 microns width. Its primary constituent, haemoglobin, enables it to carry oxygen from the lungs to the tissues and carbon dioxide from the tissues to the lungs. The red blood cell originates in the

marrow and has a life span of 100-120 days. The cell membrane weakens to such an extent by this time that it ruptures when the cell attempts to squeeze through a capillary. This process is called haemolysis. Abnormal haemolysis occurs when for some reason the red blood cells are not living the required time and they become deficient in the blood.

The white blood cell is 8-15 microns in diameter and is active in the protection of the body from disease and injury.

The platelets, 2-4 microns in diameter, are the smallest of the formed elements. Platelets will be attracted to the site of an injury and will attempt to mechanically block the bleeding. The platelet also plays an important role in the complex phenomenon of blood clotting. Blood usually clots when exposed to something foreign to the body or in the case of injury to the vessel walls. Thrombosis, or intravascular blood clotting, may be caused by an abnormally high platelet count.

In a cubic millimeter of whole blood there are approximately 5.5 million red blood cells, 5,000-10,000 white blood cells, and 250,000-400,000 platelets. The haematocrit is defined as the volume percentage of blood that is formed elements. In a normal human male, the haematocrit is 46%.

Whitmore [4] states that "rheologically speaking, mammalian blood is best described as a Bingham plastic". He notes that blood viscosity is a function of the haematocrit and the size of the vessel in which the blood is flowing. However, Kuchar and Ostrach [1] report that the viscosity of blood is essentially constant at shear rates

greater than 60 sec.$^{-1}$. Therefore, if the haematocrit is assumed constant, shear rates of greater than 60 sec.$^{-1}$ are assumed, and only tubes of diameters at least ten times greater than the red cell diameters (greater than about 0.1 mm.) are considered, blood can be said to behave as a Newtonian fluid.

1.3 Literature Survey

One of the early students of blood flow was the French physician Poiseuille. The complexities of the cardiovascular system so frustrated Poiseuille that he turned to the study of fully-developed, non-periodic flows of simpler fluids in straight rigid tubes.

By considering fully-developed flows only, Poiseuille's analysis could encompass only that portion of the flow field distant from the ends of the tube where end effects were negligible. Atabek [6] considered these end effects in developing an inlet length theory for periodic flow in tubes with rigid walls.

Kuchar and Ostrach [1] considered entrance effects associated with laminar flows of viscous fluids in circular elastic tubes. Of particular interest was their derivation of the significant dimensionless parameters. Chapter II of this thesis reviews this derivation.

Despite considerable simplification, analyses of blood flow in straight vessels continue to be extremely complex. Consequently, researchers examining flow in the more complex case of branched vessels usually have done so with the help of an experimental model rather than adopting a purely theoretical approach.

Evans et al [7] made one of the earlier attempts to analyze reflection of pulse waves which are thought to be caused partly by the branching of the cardiovascular system. Comparisons were made between the degree of reflection in a model and in an animal. Malindzak [8] and Cox [9] subsequently made more sophisticated analyses of this phenomenon.

Krovetz [10] considered the effect on haemodynamic stability (transition from laminar to turbulent flow and vice-versa) of vessel branching. He compared the critical Reynolds number in straight and branched tubes. The critical Reynolds numbers in branched tubes were considerably smaller and appeared to be independent of the varying angles of branching.

Schneck and Gutstein [11] determined the threshold flow rates at which separation occurred for various angles of branching. The severity of the separated flow condition was found to be an inverse function of the angle of branching. Schneck and Gutstein [11] noted that a direct correlation has been shown between the incidence of atherosclerotic plaque formation and the angle of bending and branching. Since an important characteristic of separated flow is its ability to injure the lining of the vessel within which the fluid flows, this separated flow condition could cause injuries to arterial linings. These injuries may in turn become sites of plaque formation.

In their review of blood flow devices, Kuchar and Scala [2] noted that "experiments on a variety of geometries have shown that the

presence of turbulence is associated with accelerated haemolysis rates. Also, they reported that stagnant regions make blood susceptible to thrombus formation.

Mitchell and Schwartz [5] noted that evidence exists which suggests there may be a correlation between turbulent blood flow, thrombosis, and the subsequent development of arterial lesions. It has been shown that plaque formation favours locations like the right angle branches of the aorta where turbulence is likely to occur. Kuchar and Ostrach [1], however, feel that turbulent flow occupies a relatively small portion of the flow cycle and they have neglected it for the purpose of their analysis.

1.4 Objectives of the Thesis

The primary objective of this thesis is to investigate the effect of varying the significant dimensionless parameters on the manner in which the flow divides at a bifurcation. The significant parameters will be either derived or explained in Chapters II and III. Also in Chapter III, the ranges of study for these parameters will be developed and the experimental apparatus devised to simulate these ranges will be described.

Some qualitative observations of flow characteristics in a bifurcation will be made. The presence or absence of such things as separation, turbulence, and stagnant regions will be noted.

CHAPTER II

THE MATHEMATICAL MODEL

2.1 Introductory Remarks

There are five significant dimensionless parameters to be considered when studying a bifurcation in the large arterial system. Three of these - the angle of branching, the ratio of branch diameters, and the normalized velocity fluctuation, all of which will be explained in Chapter III - can be either observed physically or deduced by common sense. However, the two other parameters - the Reynolds number and the unsteadiness parameter - are not so readily evident and must be derived mathematically.

Kuchar and Ostrach [1] derive these two parameters while studying blood flow in a straight non-branching tube. This chapter is primarily a resumé of those portions of their work related to the derivation of these parameters.

2.2 Simplifications Employed in the Mathematical Model

Some of the complexities of the physiological system have been outlined in Chapter I. To encompass all of these things into a mathematical model would be a monumental task indeed. Consequently the following simplifications have been made:

1. Blood is considered to be a homogeneous incompressible Newtonian fluid with a constant viscosity.

2. The vessel will be considered to be straight and circular in cross-section.

3. The entire system will be assumed to be axisymmetric; that is, all physical quantities are assumed to be independent of azimuthal position.

4. The tube will be considered semi-infinite in its longitudinal extent; that is, reflections due to smaller vessels downstream are neglected.

5. It is assumed that no side vessels branch from the tube under consideration.

6. The flow is assumed to be completely laminar in character.

7. The fluid velocity profile in the entrance cross-section is assumed to be independent of the azimuthal coordinate and always non-negative.

8. The tube walls will be considered purely elastic.

9. The Young's Modulus and Poisson's Ratio will be considered to be constant, being evaluated at a mean stress level.

10. The tube will be considered to be externally constrained in such a manner that no longitudinal displacement or motion of the tube wall occurs.

11. The radial displacement of the wall during motion is assumed to be small in comparison to the mean tube radius.

12. It is assumed that the tube is either clamped ("built-in") or simply supported at the entrance cross-section. The "clamped" as-

sumption implies that at the entrance of the tube the wall displacement is some fixed value and the rate of change of the displacement with respect to the longitudinal coordinate is zero. The "simply-supported" assumption implies that at the tube entrance the wall displacement is fixed and the bending moment is zero.

13. All effects of the gravitational body force will be neglected.

This model applies to the macrocirculation (large arteries and veins), but not to the microcirculation (arterioles, capillaries, and venules).

2.3 Derivation of the Parameters

The cylindrical polar coordinate system is employed as indicated in Figure 2.1.

The continuity equation can be expressed in general as follows:

$$\frac{\partial \rho_f}{\partial t} + \rho_f \, \mathrm{div}(\bar{q}) + \bar{q} \cdot \mathrm{grad}\,(\rho_f) = 0 \qquad (2.1)$$

where ρ_f is the fluid density, t denotes time, and $\bar{q}$ is the fluid velocity. Writing out the divergence and gradient operators in cylindrical coordinates and applying the conditions of incompressible flow (ρ_f = constant) and axial symmetry ($w = \frac{\partial}{\partial \phi} = 0$), the equation reduces to:

$$\frac{\partial u}{\partial x} + \frac{\partial v}{\partial r} + \frac{v}{r} = 0 \qquad (2.2)$$

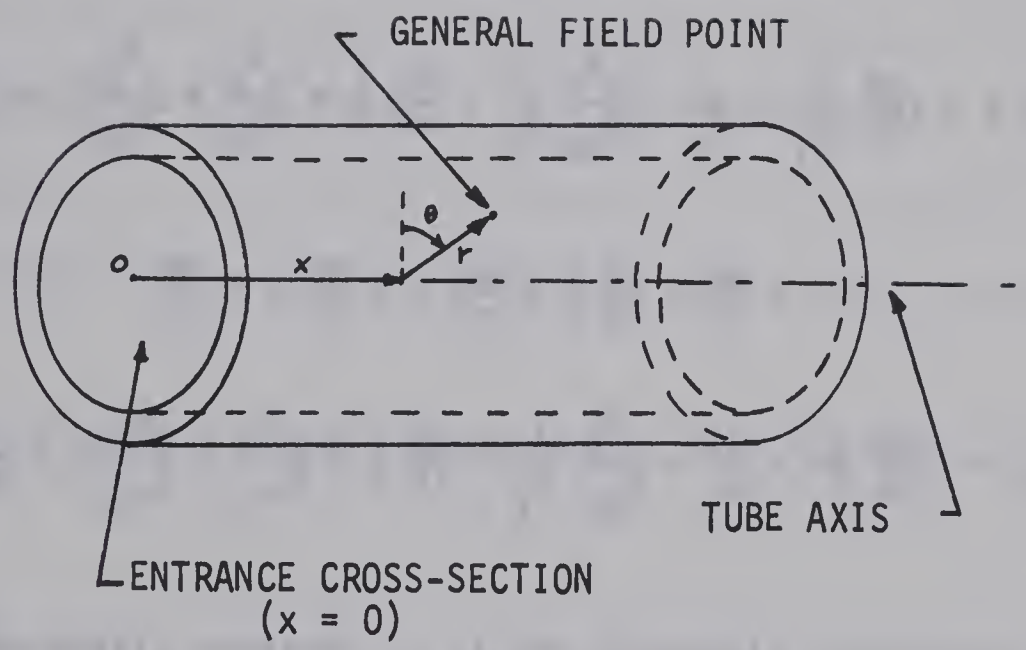

FIGURE 2.1 THE COORDINATE SYSTEM

The Navier-Stokes equations written for an incompressible fluid with constant viscosity are as follows:

$$\frac{\partial u}{\partial t} + u\frac{\partial u}{\partial x} + v\frac{\partial u}{\partial r} + \frac{w}{r}\frac{\partial u}{\partial \phi} = -\frac{1}{\rho_f}\frac{\partial p}{\partial x}$$

$$+\nu\left[\frac{\partial^2 u}{\partial x^2} + \frac{\partial^2 u}{\partial r^2} + \frac{1}{r}\frac{\partial u}{\partial r} + \frac{1}{r^2}\frac{\partial^2 u}{\partial \phi^2}\right] + F_x(m)$$

$$\frac{\partial v}{\partial t} + u\frac{\partial v}{\partial x} + v\frac{\partial v}{\partial r} + \frac{w}{r}\frac{\partial v}{\partial \phi} - \frac{w^2}{r} =$$

$$-\frac{1}{\rho_f}\frac{\partial p}{\partial r} + \nu\left[\frac{\partial^2 v}{\partial x^2} + \frac{\partial^2 v}{\partial r^2} + \frac{1}{r}\frac{\partial v}{\partial r} + \frac{1}{r^2}\frac{\partial^2 v}{\partial \phi^2} - \frac{v}{r^2} - \frac{2}{r^2}\frac{\partial w}{\partial \phi}\right] + F_r(m)$$

$$\frac{\partial w}{\partial t} + u\frac{\partial w}{\partial x} + v\frac{\partial w}{\partial r} + \frac{w}{r}\frac{\partial w}{\partial \phi} + \frac{vw}{r} =$$

$$-\frac{1}{\rho_f}\frac{\partial p}{r\partial \phi} + \nu\left[\frac{\partial^2 w}{\partial x^2} + \frac{\partial^2 w}{\partial r^2} + \frac{1}{r}\frac{\partial w}{\partial r} + \frac{1}{r^2}\frac{\partial^2 w}{\partial \phi^2} - \frac{w}{r^2} + \frac{2}{r^2}\frac{\partial v}{\partial \phi}\right] + F_\phi(m) \quad (2.3)$$

Where p is the static pressure, ν is the kinematic viscosity, and $F_x(m)$, $F_r(m)$, and $F_\phi(m)$ are the longitudinal, radial, and azimuthal components of the applied body force per unit mass of fluid.

Employing axial symmetry ($w = \frac{\partial}{\partial \phi} = 0$) and the zero-body force condition, the equations reduce to the following:

$$\frac{\partial u}{\partial t} + u\frac{\partial u}{\partial x} + v\frac{\partial u}{\partial r} = -\frac{1}{\rho_f}\frac{\partial p}{\partial x} + \nu\left[\frac{\partial^2 u}{\partial x^2} + \frac{\partial^2 u}{\partial r^2} + \frac{1}{r}\frac{\partial u}{\partial r}\right] \quad (2.4)$$

$$\frac{\partial v}{\partial t} + u\frac{\partial v}{\partial x} + v\frac{\partial v}{\partial r} = -\frac{1}{\rho_f}\frac{\partial p}{\partial r} + \nu\left[\frac{\partial^2 v}{\partial x^2} + \frac{\partial^2 v}{\partial r^2} + \frac{1}{r}\frac{\partial v}{\partial r} - \frac{v}{r^2}\right] \quad (2.5)$$

Detailed derivations and discussions of the continuity and Navier Stokes equations are given by Schlichting [12].

Further simplifications of the Navier-Stokes Equations, (2.4) and (2.5), can now be undertaken. Various strictly physical arguments can be made to determine which components of these equations are important and which are not. However, the derivation of the significant non-dimensional parameters, rather than the actual solution of the Navier-Stokes equations themselves, is of greater importance for this thesis. Consequently, these physical arguments will be bypassed and a more formal and rigorous non-dimensionalization and ordering technique will be used.

The following non-dimensionalizing transformations will be used:

$$\begin{aligned} u &= U\bar{u} & x &= L\bar{x} \\ v &= V\bar{v} & t &= T_o\bar{t} \\ r &= R_o\bar{r} & P &= (\Delta P)\,\bar{P} \end{aligned} \quad (2.6)$$

where the barred quantities are non-dimensional and U is taken as the average velocity in the longitudinal direction, V the reference radial velocity, R_o the unstressed tube radius, L the approximate length of the entrance region, ΔP the average pressure drop in the entrance

region, and T_o the period for one pulse.

Introducing these quantities into the continuity equation, (2.2), and the Navier-Stokes equations, (2.4) and (2.5), yields the following set:

$$\frac{\partial \bar{u}}{\partial \bar{x}} + \left(\frac{VL}{UR_o}\right)\left(\frac{\partial \bar{v}}{\partial \bar{r}} + \frac{\bar{v}}{\bar{r}}\right) = 0 \tag{2.7}$$

$$\left(\frac{L}{UT_o}\right)\frac{\partial \bar{u}}{\partial \bar{t}} + \bar{u}\frac{\partial \bar{u}}{\partial \bar{x}} + \left(\frac{VL}{UR_o}\right)\bar{v}\frac{\partial \bar{u}}{\partial \bar{r}} = -\left(\frac{\Delta P}{\rho_f U^2}\right)\frac{\partial \bar{P}}{\partial \bar{x}}$$

$$+ \left(\frac{\nu}{UR_o}\right)\left(\frac{L}{R_o}\right)\left[\left(\frac{R_o}{L}\right)^2\frac{\partial^2 \bar{u}}{\partial \bar{x}^2} + \frac{\partial^2 \bar{u}}{\partial \bar{r}^2} + \frac{1}{\bar{r}}\frac{\partial \bar{u}}{\partial \bar{r}}\right] \tag{2.8}$$

$$\left(\frac{V}{U}\right)\left[\left(\frac{L}{UT_o}\right)\frac{\partial \bar{v}}{\partial \bar{t}} + \bar{u}\frac{\partial \bar{v}}{\partial \bar{x}} + \left(\frac{VL}{UR_o}\right)\bar{v}\frac{\partial \bar{v}}{\partial \bar{r}}\right] = -\left(\frac{L}{R_o}\right)\left(\frac{\Delta P}{\rho_f U^2}\right)\frac{\partial \bar{P}}{\partial \bar{r}}$$

$$+ \left(\frac{V}{U}\right)\left(\frac{\nu}{UR_o}\right)\left(\frac{L}{R_o}\right)\left[\left(\frac{R_o}{L}\right)^2\frac{\partial^2 \bar{v}}{\partial \bar{x}^2} + \frac{\partial^2 \bar{v}}{\partial \bar{r}^2} + \frac{1}{\bar{r}}\frac{\partial \bar{v}}{\partial \bar{r}} - \frac{\bar{v}}{\bar{r}^2}\right] \tag{2.9}$$

In order to make both terms of the non-dimensionalized continuity equation, (2.7), of the same order, set the factor (VL/UR_o) equal to one. This yields the following relationship:

$$\frac{V}{U} = \frac{R_o}{L} \tag{2.10}$$

Substituting (2.10) in (2.8) and (2.9) yields the following:

$$\left(\frac{L}{UT_o}\right)\frac{\partial \bar{u}}{\partial \bar{t}} + \bar{u}\frac{\partial \bar{u}}{\partial \bar{x}} + \bar{v}\frac{\partial \bar{u}}{\partial \bar{r}} = -\left(\frac{\Delta P}{\rho_f U^2}\right)\frac{\partial \bar{P}}{\partial \bar{x}} +$$

$$\left(\frac{\nu}{UR_o}\right)\left(\frac{L}{R_o}\right)\left[\left(\frac{R_o}{L}\right)^2\frac{\partial^2 \bar{u}}{\partial \bar{x}^2} + \frac{\partial^2 \bar{u}}{\partial \bar{r}^2} + \frac{1}{r}\frac{\partial \bar{u}}{\partial \bar{r}}\right] \qquad (2.11)$$

$$\left(\frac{R_o}{L}\right)\left[\left(\frac{L}{UT_o}\right)\frac{\partial \bar{v}}{\partial \bar{t}} + \bar{u}\frac{\partial \bar{v}}{\partial \bar{x}} + \bar{v}\frac{\partial \bar{v}}{\partial \bar{r}}\right] = -\left(\frac{L}{R_o}\right)\left(\frac{\Delta P}{\rho_f U^2}\right)\frac{\partial \bar{P}}{\partial \bar{r}}$$

$$+ \left(\frac{\nu}{UR_o}\right)\left[\left(\frac{R_o}{L}\right)^2\frac{\partial^2 \bar{v}}{\partial \bar{x}^2} + \frac{\partial^2 \bar{v}}{\partial \bar{r}^2} + \frac{1}{r}\frac{\partial \bar{v}}{\partial \bar{r}} - \frac{\bar{v}}{\bar{r}^2}\right] \qquad (2.12)$$

Equations (2.11) and (2.12) indicate the following set of non-dimensional parameters:

$$\text{Strouhal No. (Str)} = \frac{L}{UT_o}$$

$$\text{Euler No.} = \frac{\Delta P}{\rho_f U^2}$$

$$\text{Reynold's Number (Re)} = \frac{UR_o}{\nu} \qquad (2.13)$$

$$\text{Length Ratio (Le)} = \frac{R_o}{L}$$

The Strouhal number is a measure of the importance of the unsteady effects in the flow. The Euler number represents the ratio of the pressure forces to the convective inertia forces acting on a fluid particle. The Reynolds number represents the ratio of the convective inertia forces to the viscous forces acting on a fluid particle. The length ratio is the ratio of the characteristic lengths in the radial

and axial directions.

The Navier Stokes equations can now be further simplified by determining the orders of magnitude of these parameters using compiled physiological data. However, these non-dimensional parameters are all that is required for this thesis. Consequently, the further possible simplifications will be deleted.

As pressure measurements were not a part of the experiments of this thesis, the Euler number will not be considered. Rather than considering the three remaining non-dimensional parameters separately, Kuchar and Scala [2] considered the Reynolds number and the unsteadiness parameter (a combination of the Reynolds number, the Strouhal number, and the length ratio). The unsteadiness parameter, a, is developed as follows:

$$a = \sqrt{Re \times Str \times Le}$$

$$= \sqrt{\frac{UR_o}{\nu} \frac{L}{UT_o} \frac{R_o}{L}}$$

$$a = R_o \sqrt{\frac{1}{\nu T_o}} \tag{2.14}$$

The pulse rate ω equals $1/T_o$. Consequently equation (2.14) becomes:

$$a = R_o \sqrt{\frac{\omega}{\nu}} \tag{2.15}$$

The validity of the non-dimensional parameters will not be damaged by substituting the unstressed diameter of the vessel D for the unstressed radius R_o. Therefore, two of the pertinent dimensionless parameters to be considered are as follows:

$$Re = \frac{UD}{\nu} \tag{2.16}$$

and

$$a = D \sqrt{\frac{\omega}{\nu}} \tag{2.17}$$

It should be noted that the Reynolds number (Re) is calculated at the entrance to the bifurcation.

CHAPTER III

THE EXPERIMENTAL MODEL

3.1 The Range of Study

The Reynold's number Re and unsteadiness parameter a as described by equations (2.16) and (2.17) have now been developed. It is now necessary to determine the range of these parameters for the physiological case. To do this, the following data has been gleaned from Wintrobe [13], Tuttle and Schottelius [14], and Bell, Davidson, and Scarborough [15]:

1. The relative viscosity of blood with respect to distilled water varies from 3.5 to 5.4.
2. Blood density varies from 1.048 to 1.066 gm/cm^3.
3. The kinematic viscosity of distilled water equals .010027 cm^2/sec.
4. For an "average" case, blood will flow at a velocity of 32 cm/sec through an aorta of 2.1 cm diameter.
5. Human pulse rate varies from 50 to 100 beats per minute.
6. The diameter of the human aorta varies from 1.5 to 2.1 cm.

Substitution of this data into equations (2.16) and (2.17) yields the following ranges of study:

$$1300 < Re < 2040 \tag{3.1}$$

$$6 < a < 15 \tag{3.2}$$

The flow from the heart will be approximated as a sinusoidal-type flow as illustrated in Figure 3.1. The normalized velocity fluctuation λ is defined by the following expression:

$$\lambda = \frac{U'}{U} \tag{3.3}$$

where U is the mean velocity and U' is the fluctuating component of velocity. Kuchar and Scala [2] report the physiological range for λ to be as follows:

$$1 < \lambda < 2 \tag{3.4}$$

The blood vessels of the body branch in many ways. This work will be confined to the case of a side branch off a straight vessel as illustrated in Figure 3.2. Consideration of this bifurcation geometry gives rise to two further dimensionless parameters - the angle between the branches, θ, and the ratio of the branch diameters, β, as defined by:

$$\beta = \frac{d}{D} \tag{3.5}$$

where D is the internal diameter of the mainline branch which is the

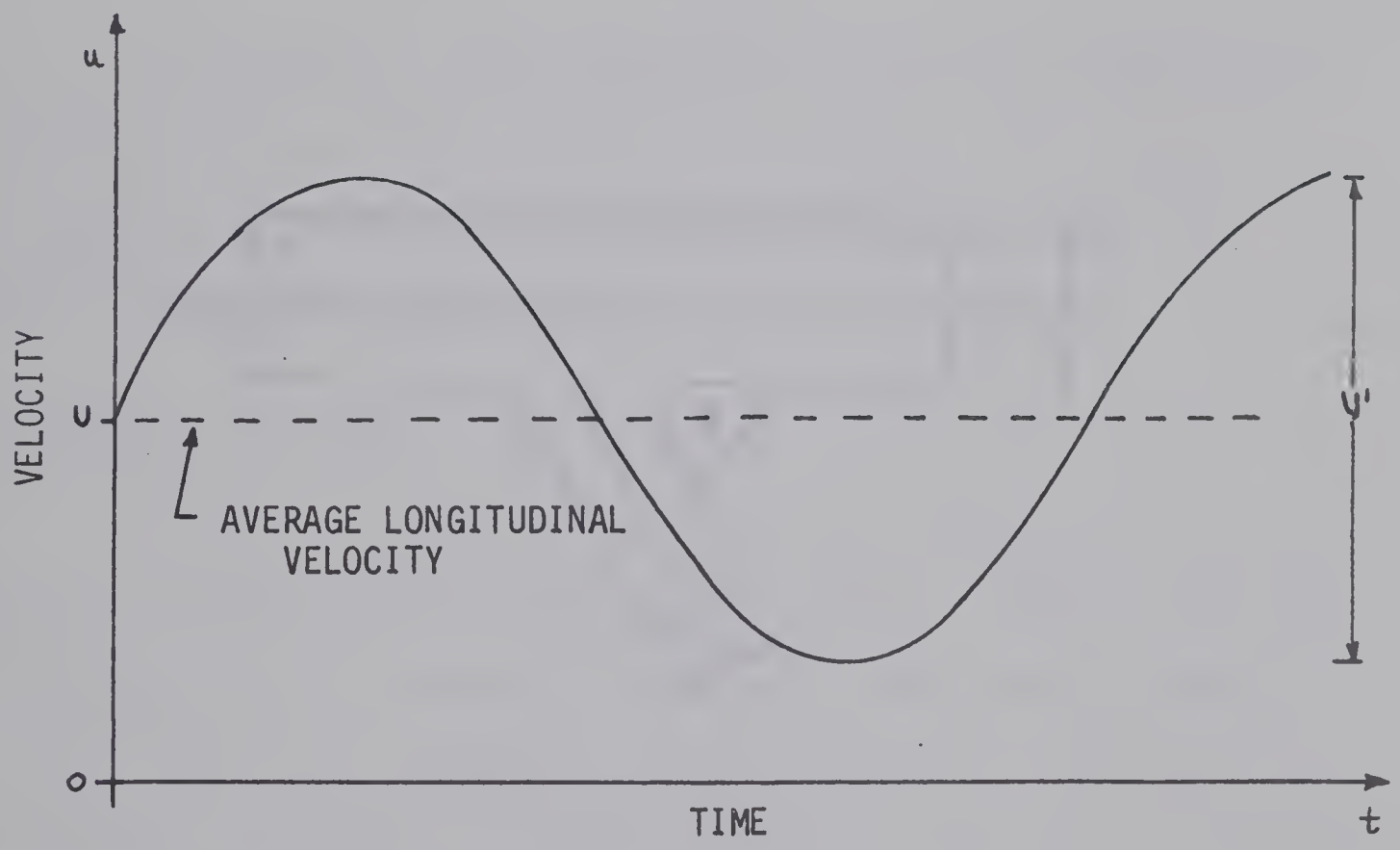

FIGURE 3.1 EXPERIMENTAL SIMULATION OF FLOW FROM THE HEART

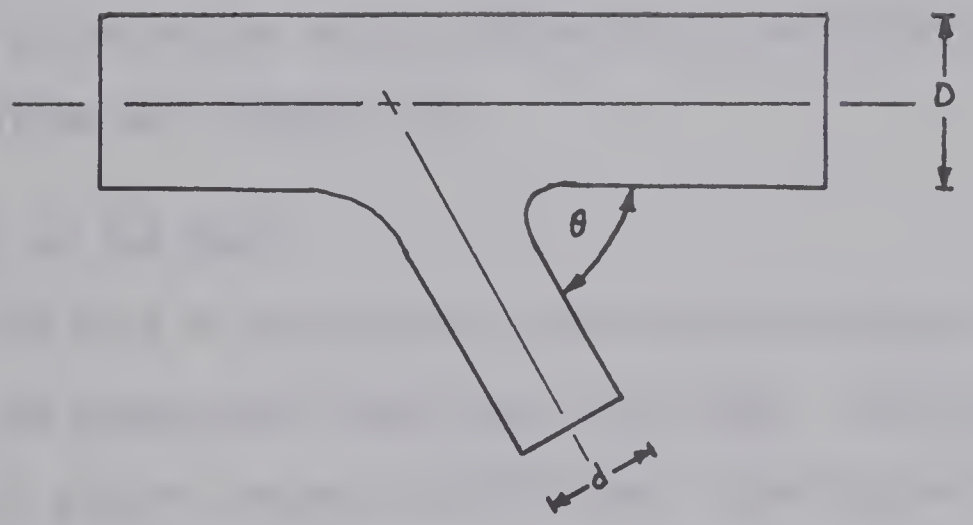

FIGURE 3.2 THE EXPERIMENTAL BIFURCATION

same up and downstream of the bifurcation and d is the internal diameter of the side-branch. The ranges of study for θ and β have been chosen as follows:

$$30° \leq \theta \leq 90° \tag{3.6}$$

$$0.20 \leq \beta \leq 0.80 \tag{3.7}$$

The range for θ was suggested by Dr. R.D. Laurenson of the Department of Anatomy at the University of Alberta. The range for β was chosen by the author after examination of photographs of the arterial system (eg. Figure 1.2).

3.2 Design of the Model

For ease of observation, the internal diameter of the main branch of the experimental model was 1.25 inches. Weiting [16] found that a 36.7% glycerol-aqueous solution was a good hydraulic analogue for blood. The specific gravity of this mixture is 1.10 and the viscosity is 4.5 centepoise. The calculations of these quantities are in Appendix A. This viscosity falls within the range accepted for human blood (3.5 to 5.4 cp.) and the specific gravity is reasonably close (1.048 to 1.066). For the purpose of flow visualization, resin particles were suspended in the blood analogue. As the specific gravity of these particles was 1.10, the glycerol-aqueous solution had to be mixed to this specific gravity for the suspension to be possible.

Substituting the kinematic viscosity of the blood analogue ($\nu = \mu/\rho_f = .045/1.10$) and the main branch diameter (D = 1.25") of the experimental model into the relationships for Reynolds number Re (2.16) and unsteadiness parameter a (2.17) yields the following relationships:

$$a = 2.03 \sqrt{\omega} \tag{3.8}$$

$$Re = 740\ Q \tag{3.9}$$

where the pulse rate ω is measured in cycles per minute and the flow rate Q is measured in gallons per minute (Imperial).

Substituting expressions (3.8) and (3.9) into (3.1) and (3.2) yields the ranges of pulse rate and flow rate the experimental model must be capable of:

$$1.76 < Q < 2.76 \tag{3.10}$$

$$8.7 < \omega < 54.6 \tag{3.11}$$

The sinusoidal flow pattern was achieved by use of a cam-driven piston/cylinder assembly which will be described in detail in Section 3.3. The required range of the normalized velocity fluctuation λ was covered by the use of cams of various sizes. In Appendix B the interdependence of the length of the piston stroke ℓ, the velocity

fluctuation λ, the flow rate Q, and the pulse rate ω is outlined. The relationship developed in Appendix B is as follows:

$$\ell = 3.5 \frac{\lambda Q}{\omega} \qquad (3.12)$$

where the length of stroke ℓ is measured in inches.

3.3 Description of the Apparatus

Figure 3.3 and 3.4 are a schematic and a photograph respectively of the experimental model.

3.3.1 The Test Section

The bifurcations were made by the University of Alberta Glass Shop. An elastic bifurcation would have been more favourable but attempts to make one by a dipping technique were not completely successful.

The technique to be employed was to dip the glass bifurcation into a liquid rubber which set when heated (the material used was the childrens' toy "Plastigoop"). The glass was then to be broken and the flexible bifurcation salvaged. This technique was tried using a length of straight glass tubing. Although it appeared that a structurally sound bifurcation could be made, it was not possible to achieve the transparency necessary for flow observation. Consequently, this technique was abandoned and glass bifurcations were used. In the interest of investigators who may attempt the construction of an elastic bifurcation in the future, the author found that a considerably better cast was taken from the inside

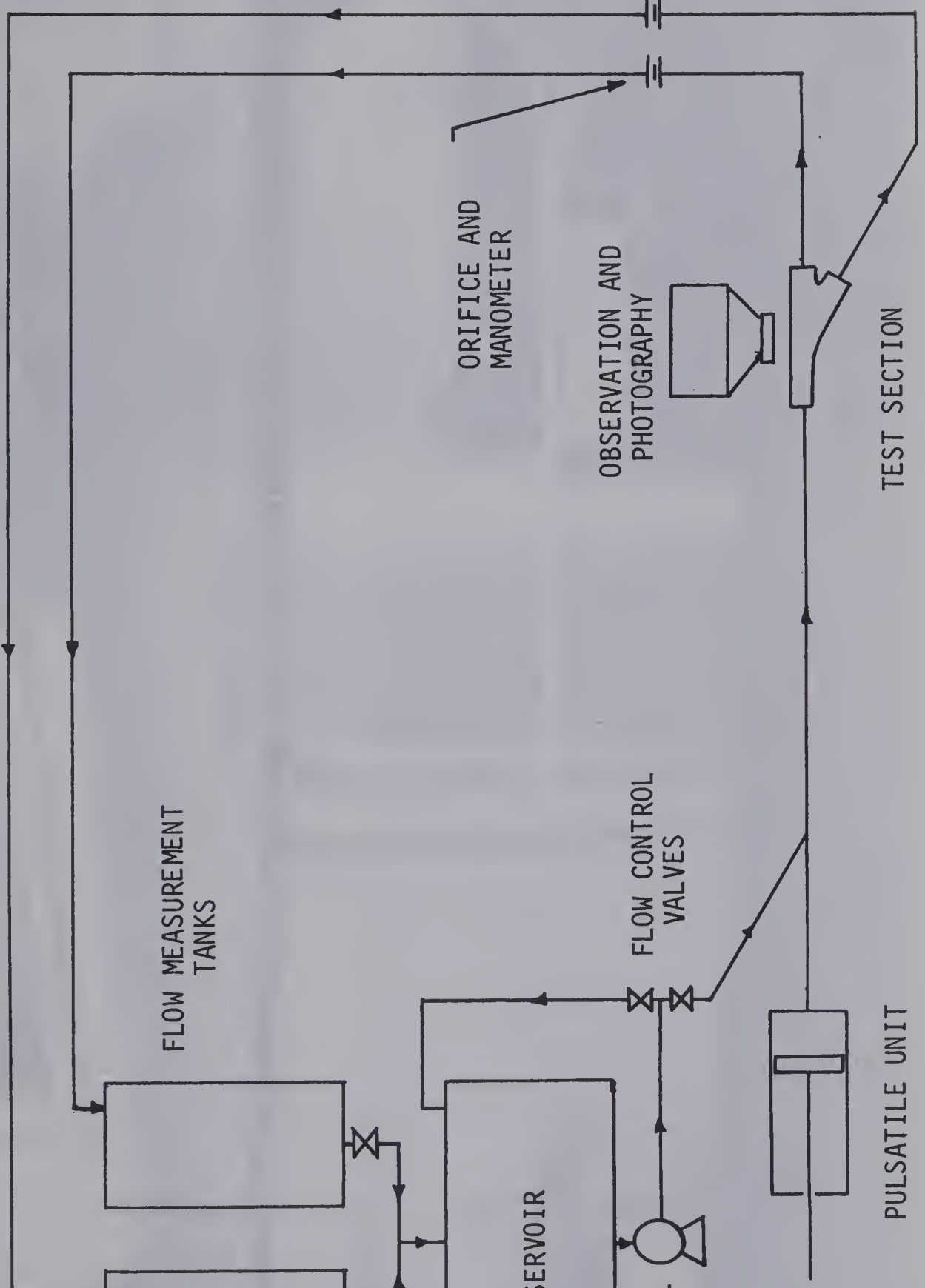

FIGURE 3.3 SCHEMATIC OF THE APPARATUS

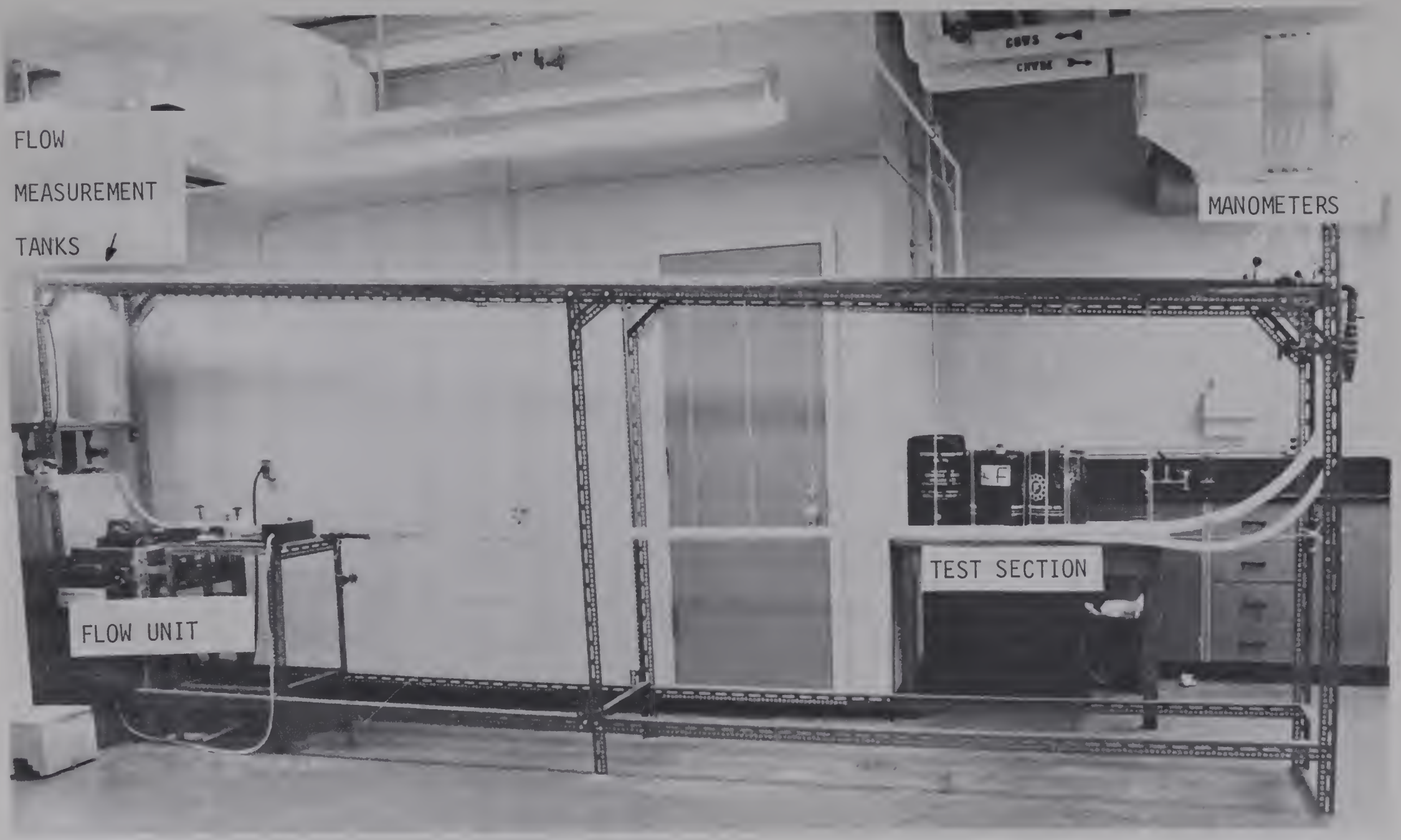

FIGURE 3.4 PHOTOGRAPH OF THE EXPERIMENTAL MODEL

of the glass tubing than from the outside.

Glass bifurcations of the following geometries were made and tested:

D(ins.)	d(ins.)	θ(degrees)
1.25	1.00	50°
1.25	0.75	30°
1.25	0.75	50°
1.25	0.75	70°
1.25	0.75	90°
1.25	0.50	50°
1.25	0.25	50°

In this way the prescribed ranges for θ and β were covered. Typical bifurcations are shown in Fig. 3.5.

The inlet and outlets to the bifurcation were surgical tubing[1] suspended by twine from a dexion frame. This method of suspension approximates the physiological case in that a certain degree of radial movement is possible. Another method considered was suspension of the test section in a bath. The former method was chosen because of its simplicity of construction and the fact that a similar apparatus has been used elsewhere (Dr. S. Ostrach, Case Institute). The upstream branch was approximately eight feet in length[1] and as straight and horizontal as possible. The downstream branches were

---

1. See Appendix E, Section E-1

FIGURE 3.5 TYPICAL GLASS BIFURCATIONS

FIGURE 3.6 PHOTOGRAPH OF THE TEST SECTION

approximately four feet in length and curved upwards from the horizontal plane of the bifurcation to the overhead return lines. Figure 3.6 is a photograph of the test section. The entrance to the upstream branch was "clamped" as defined in section 2.1. Flow visualization was by suspension of small spherical resin particles[2] as done by Weiting [16]. Flow photographs were taken with a Graflex Camera fitted with a Polaroid film unit.

3.3.2 The Flow Unit

The sinusoidal flow was obtained by using a centrifugal pump[3] in series with a cam-driven piston cylinder arrangement. The cylinder was made of 4" I.D. stainless steel pipe, both ends of which were threaded to facilitate disassembly should any repair or alteration be necessary. The piston was equipped with a leather cup seal and the cam follower was a roller-type. To cover the range of study as defined by the dimensionless parameters Re, a, and λ, various cams were used. The actual cams used are described in Chapter IV and the design of a typical cam is outlined in Appendix C.

A variable speed D.C. motor[4] was used to power the cam. To produce the desired range of pulse rate, a 30:1 worm gear reducer[5] was installed to transmit power from the motor to the cam.

The flow rate and consequently the Reynolds number was controlled by two 1/2" gate valves. One valve controlled the rate of direct return to the reservoir, and the other controlled the flow to the test section (see Figure 3.3).

Figure 3.7 is a photograph of the flow unit with a typical cam in place.

3.3.3 Miscellaneous

The flow rates in each branch were determined by simultaneously closing the drains to the flow measurement tanks and measuring the elapsed time to gather a known quantity (two gallons). These tanks were fitted with gauge glasses running their entire vertical extent. Two gallons of fluid was carefully measured and poured into each partially-full tank. The heights of the fluid in the gauge glasses before and after the two gallons addition were marked on the glasses. The initial levels of fluid in each tank were slightly staggered to enable one experimenter to measure time elapsed for both tanks simultaneously. An orifice and manometer were installed and calibrated in each line, but this method of measurement proved completely unsatisfactory for pulsatile flow. The apparatus was useful, however, for establishing the approximate desired flow rate before the pulsatile unit was engaged. The manometer calibration curves are included in Appendix D.

Bell, Davidson, and Scarborough [15] quote the mean diastolic pressure at the inlet of the aorta as 90 mm. Hg. This is equivalent to about 4 feet of blood which is the approximate vertical displacement of the inlet to the flow measurement tanks above the plane of the test section.

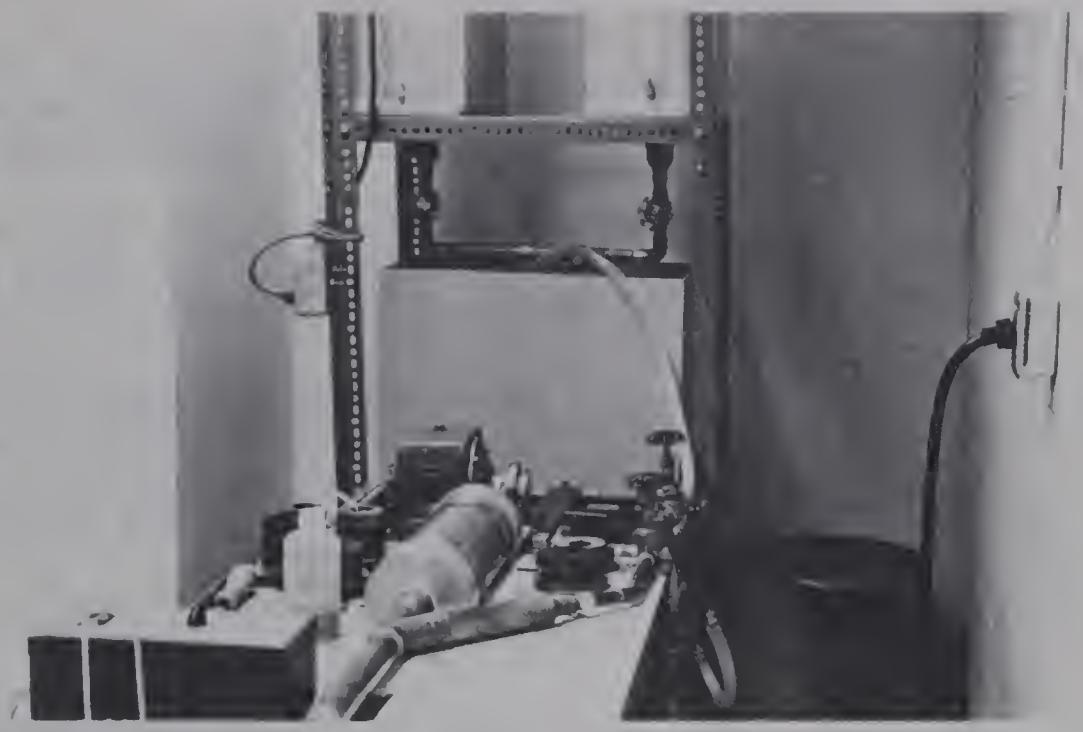

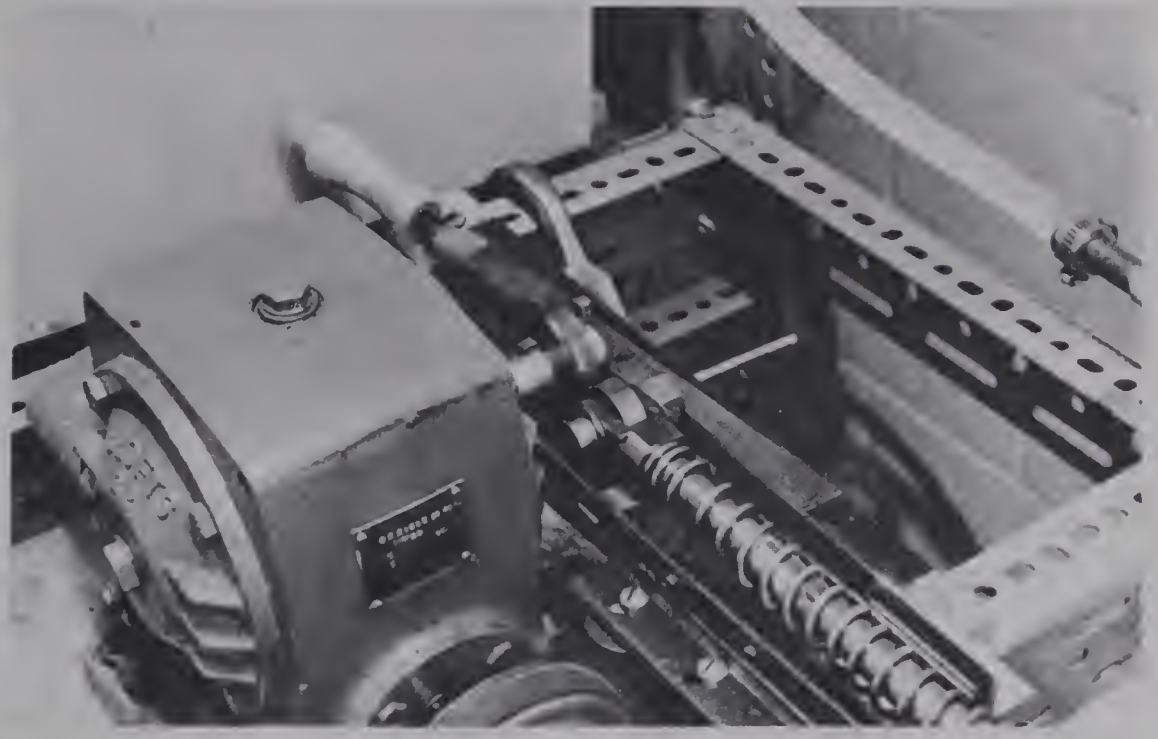

FIGURE 3.7 PHOTOGRAPHS OF THE FLOW UNIT

Footnotes - Chapter 3

1. "Jayon" Surgical Tubing
   Johnston Industrial Plastics
   Edmonton, Alberta

2. "Amberlite" Ion Exchange Resin IRA 904
   Rohm & Haas Co. of Canada Ltd.
   West Hill, Ontario

3. "Little Giant" Submersible Pump
   Model No. 3E12NR
   Electrical Industries Ltd.
   Edmonton, Alberta

4. 2 H.P. D.C. Motor
   Model GP-100
   General Electric Ltd.
   Edmonton, Alberta

5. Crofts Model 22 Worm Gear Reducer
   Renold Chains Ltd.
   Edmonton, Alberta

CHAPTER IV

THE EXPERIMENTS

4.1 Summary of Parameters and Ranges of Study

In Chapters II and III, the five significant dimensionless parameters have been developed and explained. Also, the pertinent ranges of study for these parameters have been developed and, where necessary, these ranges converted so they can be duplicated in the experimental model. This information is summarized in Table 4.1.

4.2 The Mass Flow Ratio

The Mass Flow Ratio γ is defined as the ratio of the flow rate in the side branch Q_d to the flow rate in the mainline branch Q_D. That is,

$$\gamma = \frac{Q_d}{Q_D} \tag{4.1}$$

The dependence of γ on each of the five parameters was examined. Each parameter was varied throughout its range while the other four parameters were held constant. To do this, it was necessary to match the size of the cam to the parameters by equation (3.12). Re and a were converted to their dimensional counterparts, Q and ω, by equations (3.8) and (3.9) respectively.

TABLE 4.1 THE DIMENSIONLESS PARAMETERS

AND THEIR RANGES OF STUDY

Parameter	Non-Dimensional Range of Study	Experimental Range of Study
$Re = \frac{UD}{\nu}$	$1300 < Re < 2040$	$1.76 < Q < 2.76$ (g.p.m)
$a = D \sqrt{\frac{\omega}{\nu}}$	$6 < a < 15$	$8.7 < \omega < 54.6$ (r.p.m.)[2]
$\lambda = \frac{U'}{U}$	$1 < \lambda < 2$	$1 < \lambda < 2$
$\beta = \frac{d}{D}$	$0.20 \leq \beta \leq 0.80$	$0.20 \leq \beta \leq 0.80$
θ	$30° \leq \theta \leq 90°$	$30° \leq \theta \leq 90°$

At the beginning of each experimental session, the density of the blood analogue was checked by hydrometer[1] and adjusted as required.

The experimental method was as follows:

1. If it was not already in place, the appropriate bifurcation was installed.

2. The centrifugal pump was started and the required flow rate set as closely as possible using the calibrated manometers.

3. The appropriate cam was installed.

[1] Exax Heavy Liquid Hydrometer

[2] See Appendix E, Section E-2

4. The pulsatile unit was set at the desired frequency which was checked by stopwatch.

5. The drains from the flow measurement tanks were closed simultaneously and the elapsed times to gather two gallons in each tank were measured by two stopwatches.

6. The flow rates in each branch, Q_d and Q_D, the Mass Flow Ratio γ, and the total flow Q were computed.

7. Usually, the exact total flow rate was not obtained. Instead, Q was usually slightly above or below the required value. When this occurred, the appropriate change was made in the flow rate and steps 5 and 6 repeated. In this way the required Q could be "closed in on" from above and below. The values computed for γ were close enough together that an interpolation to the correct value could be made.

Steps 1 through 7 were repeated for each experimental point obtained. Although this method proved exceedingly tedious and time consuming, it appeared to be the only method with which reasonable accuracy could be achieved.

4.2.1 The Mass Flow Ratio, γ, as a Function of the Unsteadiness Parameter, a, and the Normalized Fluctuating Component of Velocity, λ

The Reynolds number was kept constant at Re = 1630 and the bifurcation used was defined by the parameters β = 0.75"/1.25" = 0.60 and $\theta = 50°$. The dependence of γ on a was examined for λ = 1.0, 1.5, and 2.0. The size of cams used (defined by length of stroke, ℓ), the pulse rate, ω, the corresponding value for the unsteadiness parameter

a, and the experimental value obtained for the Mass Flow Ratio, γ, are given in Tables 4.2, 4.3, and 4.4. This data is illustrated in Figure 4.1.

TABLE 4.2 DEPENDENCE OF γ ON a FOR $\lambda = 1.0$

Re = 1630 (Q = 2.20 g.p.m.),

$\beta = 0.60$, $\theta = 50°$

ℓ(ins.)	ω(r.p.m.)	a	γ
2.00	3.85	3.98	0.935
1.00	7.70	5.62	0.938
0.75	10.25	6.50	0.939
0.60	12.8	7.25	0.935
0.50	15.4	7.95	0.950
0.43	17.9	8.58	0.947
0.37	20.8	9.11	0.950
0.30	25.6	10.29	0.957
0.25	30.8	11.25	0.955
0.23	33.4	11.72	0.962
0.20	38.5	12.55	0.962
0.18	42.8	13.25	0.963
0.15	51.3	14.51	0.970

For $\omega = 0$, Re = 1630, $\beta = 0.60$, $\theta = 50°$,

$\gamma = 0.937$

TABLE 4.3 DEPENDENCE OF γ ON a FOR $\lambda = 1.5$

Re = 1630 (Q = 2.20 g.p.m.), $\beta = 0.60$, $\theta = 50°$

ℓ(ins.)	ω(r.p.m.)	a	γ
2.00	5.77	4.87	0.941
1.00	11.53	6.88	0.946
0.85	13.59	7.47	0.948
0.75	15.4	7.97	0.945
0.70	16.5	8.24	0.952
0.60	19.2	8.87	0.960
0.50	23.1	9.75	0.968
0.47	24.6	10.05	0.975
0.41	28.1	10.75	0.980
0.38	30.4	11.18	0.978
0.35	33.0	11.64	0.975
0.32	37.0	12.32	0.980
0.30	38.5	12.59	0.983
0.25	46.2	13.78	0.975
0.23	50.2	14.40	0.983

TABLE 4.4 DEPENDENCE OF γ ON a FOR $\lambda = 2.0$

Re = 1630 (Q = 2.20 g.p.m.); $\beta = 0.60$, $\theta = 50°$

ℓ(ins.)	ω(r.p.m.)	a	γ
2.00	7.70	5.62	0.953
1.50	10.25	6.50	0.958
1.20	12.82	7.25	0.960
1.00	15.40	7.95	0.970
0.90	17.12	8.39	0.979
0.85	18.12	8.63	0.978
0.75	20.5	9.18	0.985
0.70	22.0	9.50	0.991
0.60	25.7	10.25	0.997
0.50	30.8	11.25	1.010
0.47	32.8	11.60	1.012
0.44	35.0	12.00	1.015
0.41	37.5	12.40	1.014
0.38	40.5	12.90	1.020
0.35	44.0	13.43	1.020
0.32	48.1	14.10	1.019
0.30	51.3	14.51	1.023

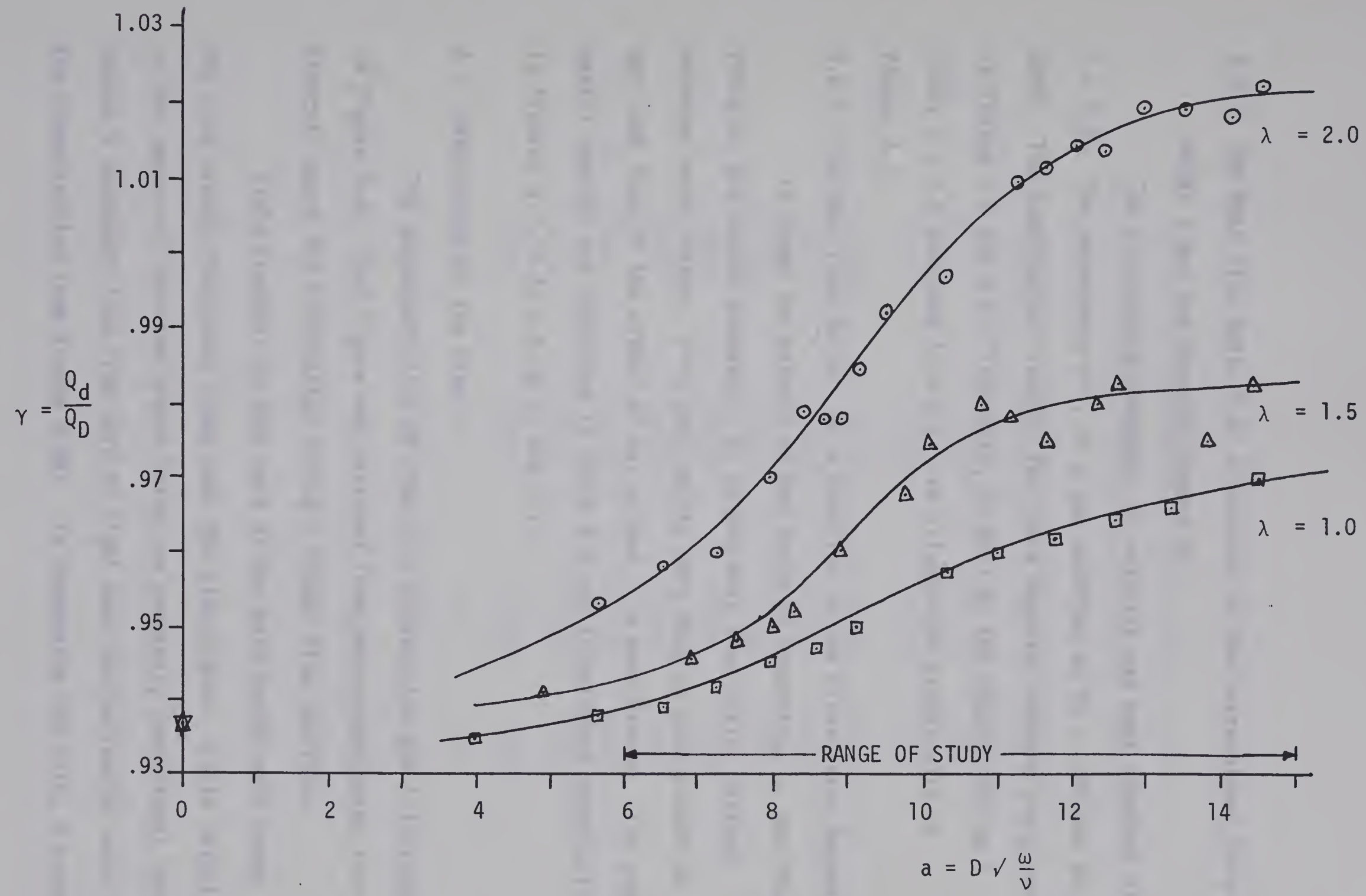

FIGURE 4.1 MASS FLOW RATIO γ vs UNSTEADINESS PARAMETER a FOR λ = 1.0, 1.5, 2.0,

$\beta = \frac{0.75}{1.25} = 0.60$; $\theta = 50°$; Re = 1630

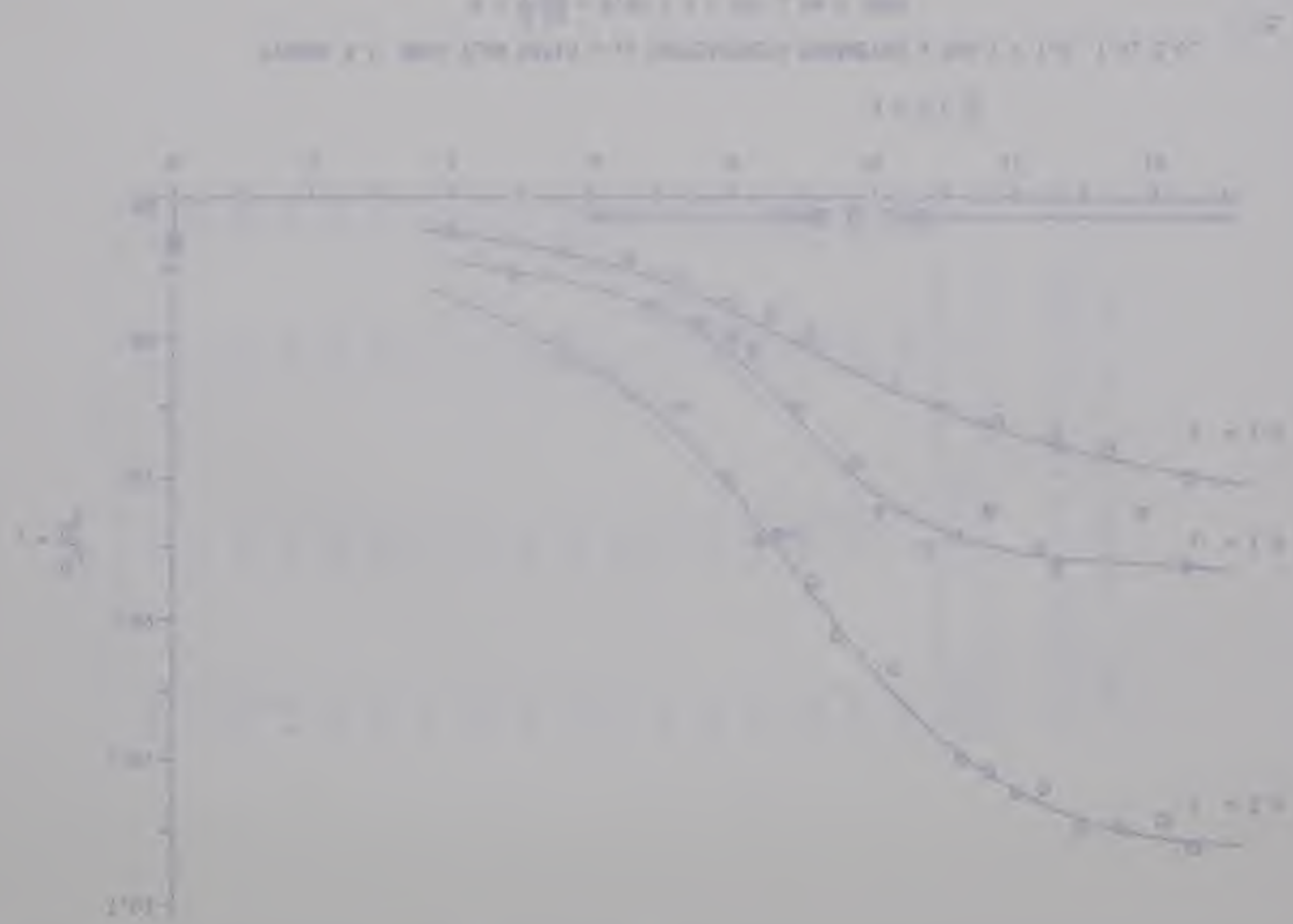

4.2.2 The Mass Flow Ratio γ as a Function of the Unsteadiness Parameter a and the Reynolds Number Re

The fluctuating component of velocity was kept constant at $\lambda = 2.0$. The dependence of γ on a was examined at Re = 1330 and Re = 2000. The experimental results for these Reynolds numbers are given in Tables 4.5 and 4.6. This data, as well as the results for Re = 1630, $\lambda = 2.0$ obtained in 4.2.1, are illustrated graphically in Figure 4.2.

4.2.3 The Mass Flow Ratio γ as a Function of the Bifurcation Geometry

To study the effects of the angle of branching, θ, and the ratio of the branch diameters, β, on the mass flow ratio, various branches were tested. Five test points were done on each branch to get some idea of the effect of Re, a, and λ in each branch. The experimental results are tabulated in Table 4.7 and illustrated graphically in Figures 4.3, 4.4, 4.5, 4.6, and 4.7.

4.3 Description of the Flow

The characteristics of flow in a bifurcation are illustrated in Figure 4.8. This figure was sketched from photographs taken from directly above the bifurcation during a steady flow condition.

Fluid proximal to that part of the main vessel wall where the side branch intersects flows down the side branch. Fluid velocity in the center of the side branch being the greatest, centrifugal force causes a secondary flow from left to right near the horizontal axis of the cross-section (see Figure 4.8b). To compensate for this, a secondary

TABLE 4.5 DEPENDENCE OF γ ON a FOR $\lambda = 2.0$

Re = 1330 (Q = 1.80 g.p.m.), $\beta = 0.60$, $\theta = 50°$

ℓ(ins.)	ω(r.p.m.)	a	γ
2.00	6.30	5.10	0.947
1.20	10.50	6.57	0.960
0.90	14.00	7.60	0.965
0.70	18.00	8.60	0.976
0.60	21.0	9.30	0.991
0.50	25.2	10.20	1.006
0.44	28.6	10.85	1.014
0.41	30.8	11.25	1.028
0.38	33.2	11.70	1.032
0.35	36.0	12.20	1.040
0.32	39.4	12.72	1.038
0.30	42.0	13.15	1.042
0.25	50.4	14.42	1.039

TABLE 4.6 THE DEPENDENCE OF γ ON a FOR $\lambda = 2.0$

Re = 2000 (Q = 2.70 g.p.m.) $\beta = 0.60$, $\theta = 50°$

ℓ(ins.)	ω(r.p.m.)	a	γ
2.00	9.45	6.23	.953
1.50	12.60	7.18	.961
1.20	15.75	8.05	.975
1.00	18.90	8.81	.980
0.90	21.00	9.30	.988
0.85	22.20	9.55	.985
0.80	23.6	9.85	.988
0.75	25.2	10.20	.986
0.70	27.0	10.51	.988
0.60	31.5	11.40	.993
0.50	37.8	12.45	.993
0.47	40.2	12.85	.994
0.44	43.0	13.30	.995
0.41	46.1	13.65	.994
0.38	49.7	14.3	.992
0.35	54.0	14.9	.993

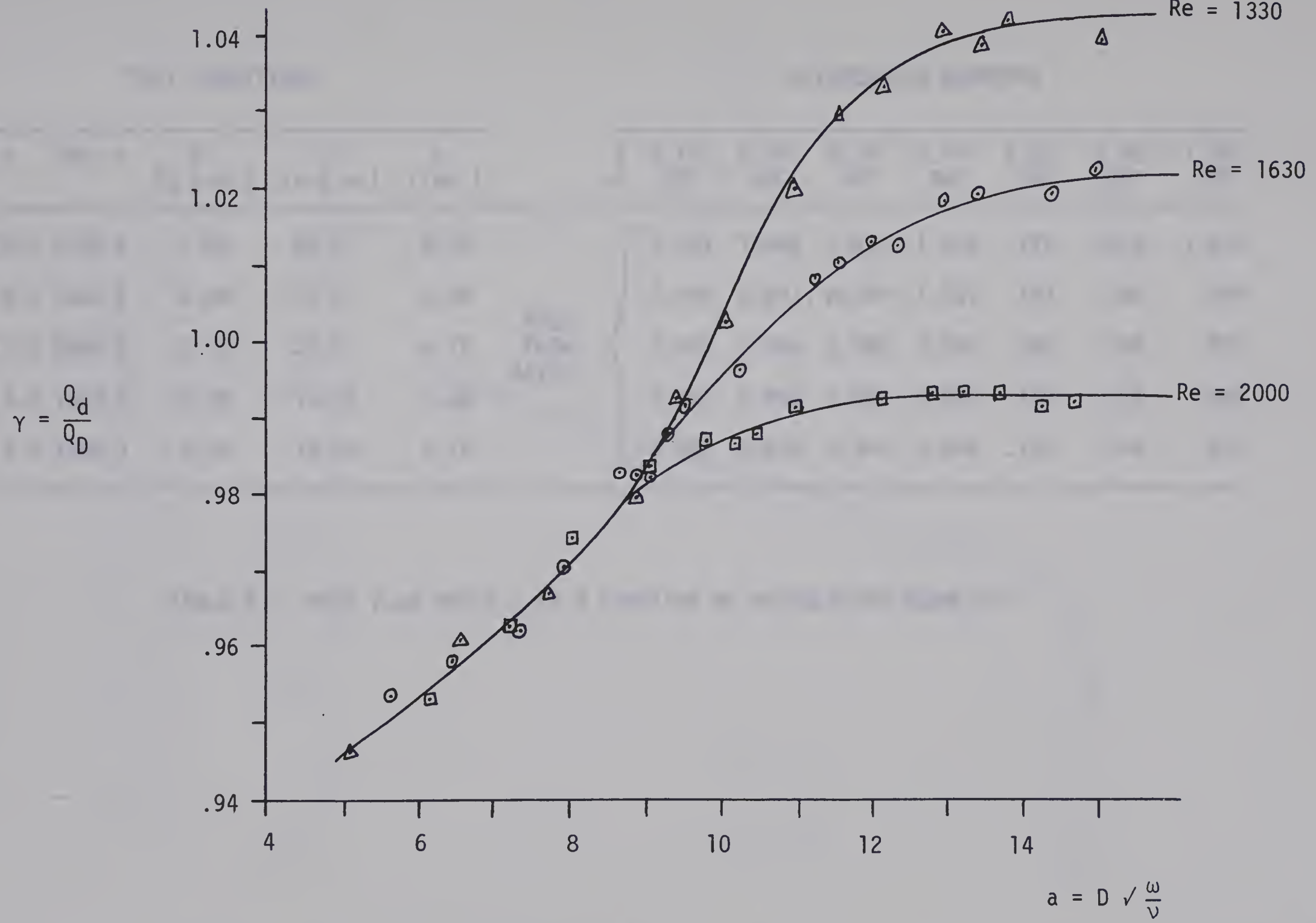

FIGURE 4.2 MASS FLOW RATIO γ AS A FUNCTION OF UNSTEADINESS PARAMETER a AND REYNOLDS NUMBER Re

$$\beta = \frac{0.75}{1.25} = 0.60 \qquad \theta = 50° \qquad \lambda = 2.0$$

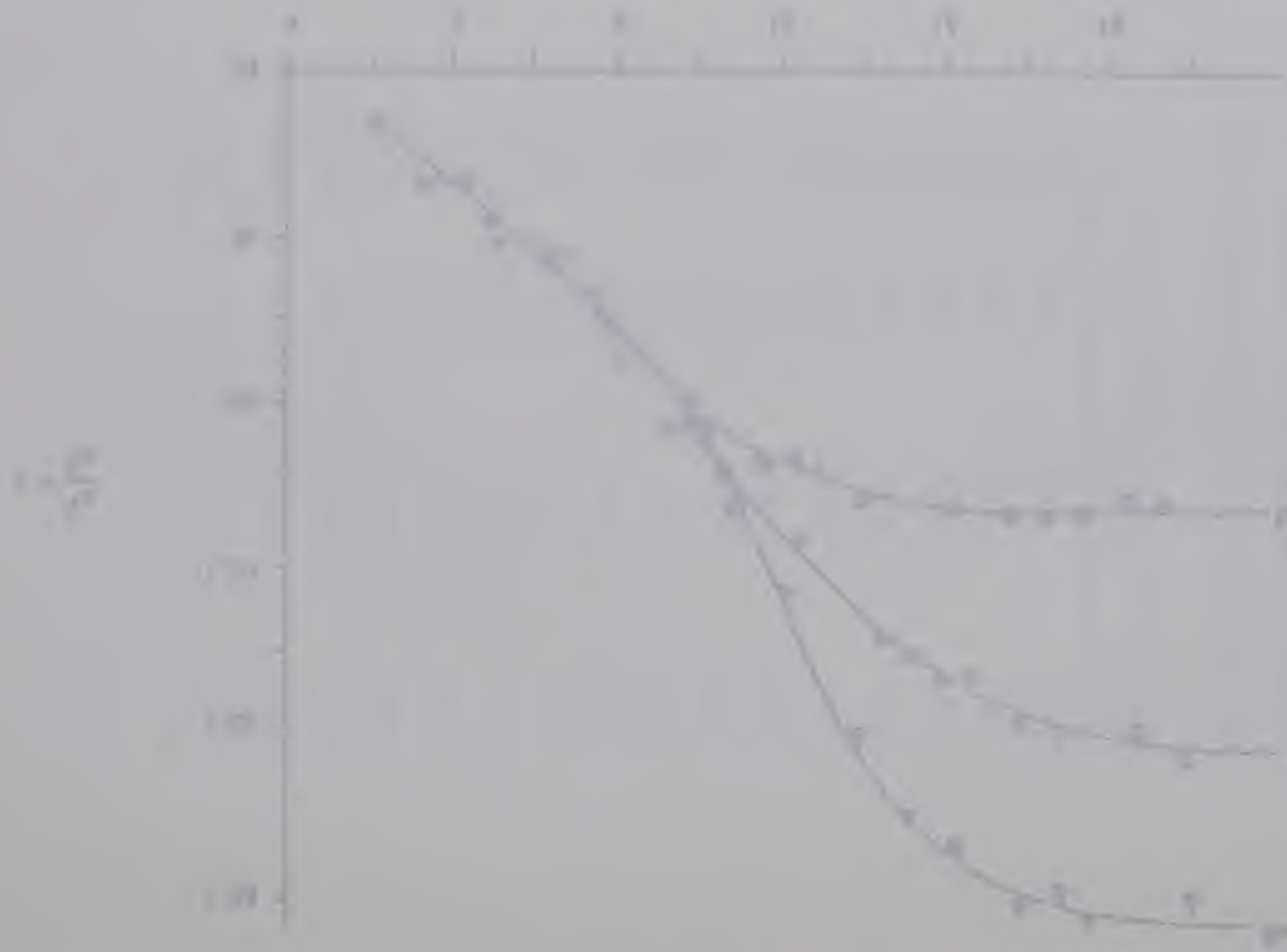

TEST CONDITIONS						BIFURCATION GEOMETRY						
a	Re	λ	Q (g.p.m.)	ω (r.p.m.)	ℓ (ins.)	d / θ	0.75" 30°	0.75" 50°	0.75" 70°	0.75" 90°	0.25" 50°	0.50" 50°	1.00" 50°
10.2	1330	2	1.80	25.2	0.50	MASS FLOW RATIOS	1.003	1.006	1.013	1.014	.174	.828	1.010
10.2	1630	2	2.20	25.2	0.60		0.995	0.997	0.994	1.001	.193	.788	.998
10.2	2000	2	2.70	25.2	0.75		0.995	0.986	0.990	0.993	.206	.796	.985
6.5	1630	2	2.20	10.25	1.50		0.964	0.958	0.965	0.968	.189	.770	.985
6.5	1630	1	2.20	10.25	0.75		0.942	0.939	0.943	0.949	.181	.740	.975

TABLE 4.7 MASS FLOW RATIO γ AS A FUNCTION OF BIFURCATION GEOMETRY

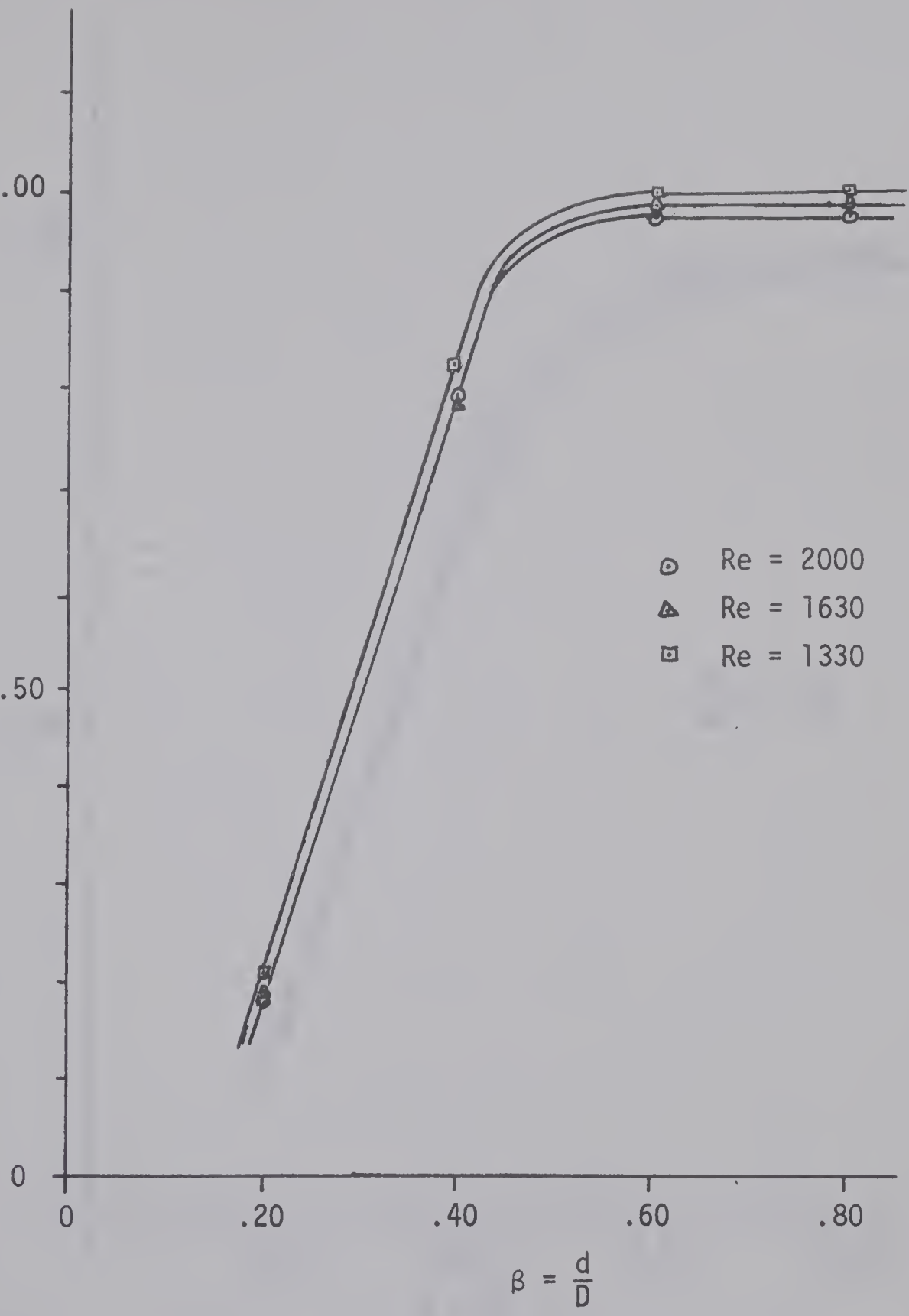

FIGURE 4.3 MASS FLOW RATIO γ vs DIAMETER RATIO β

AS A FUNCTION OF Re $\theta = 50°$, a = 10.2, $\lambda = 2.0$

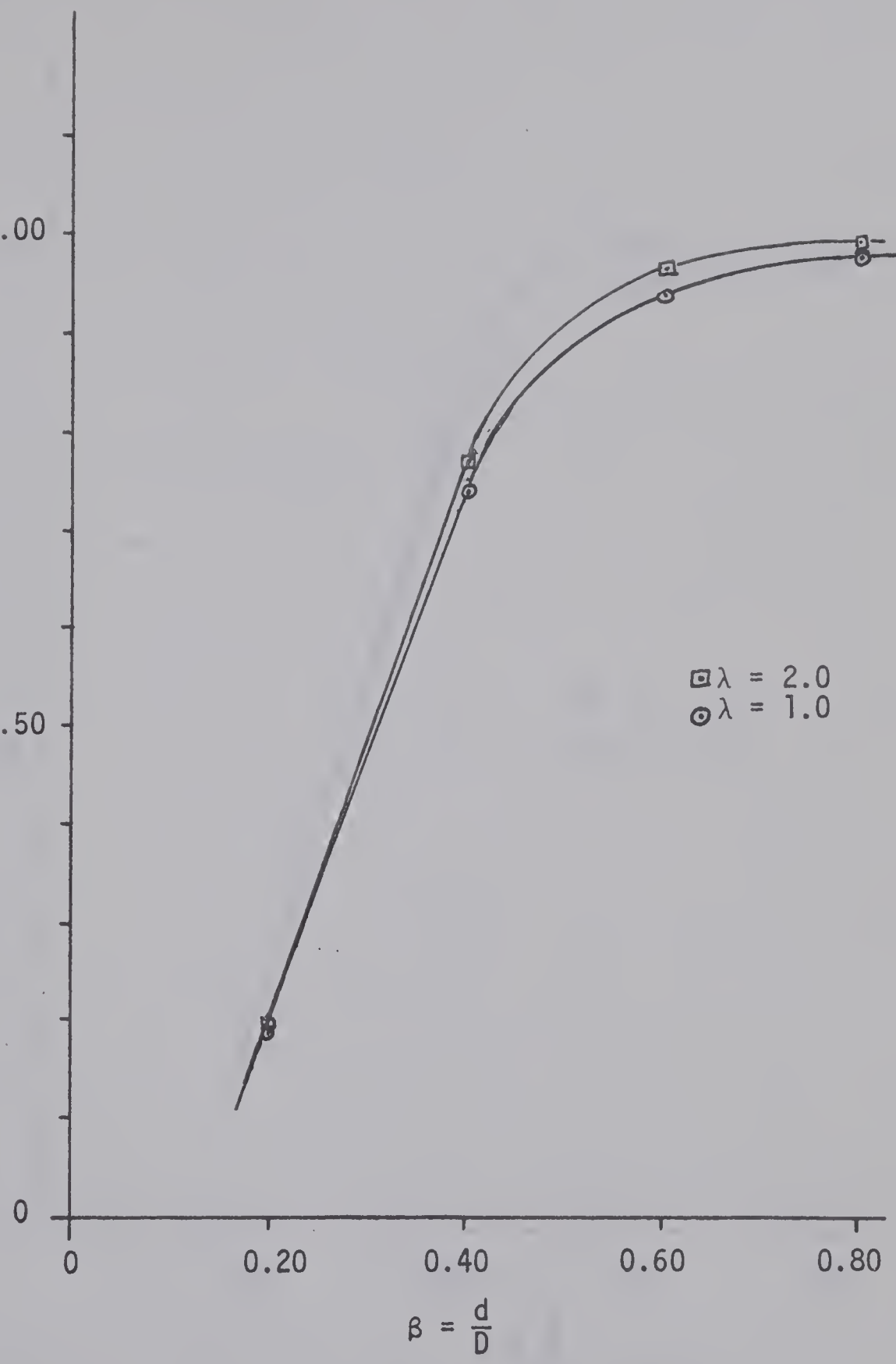

FIGURE 4.4 MASS FLOW RATIO γ vs DIAMETER RATIO β

AS A FUNCTION OF λ $\theta = 50°$ $a = 6.50$ $Re = 1630$

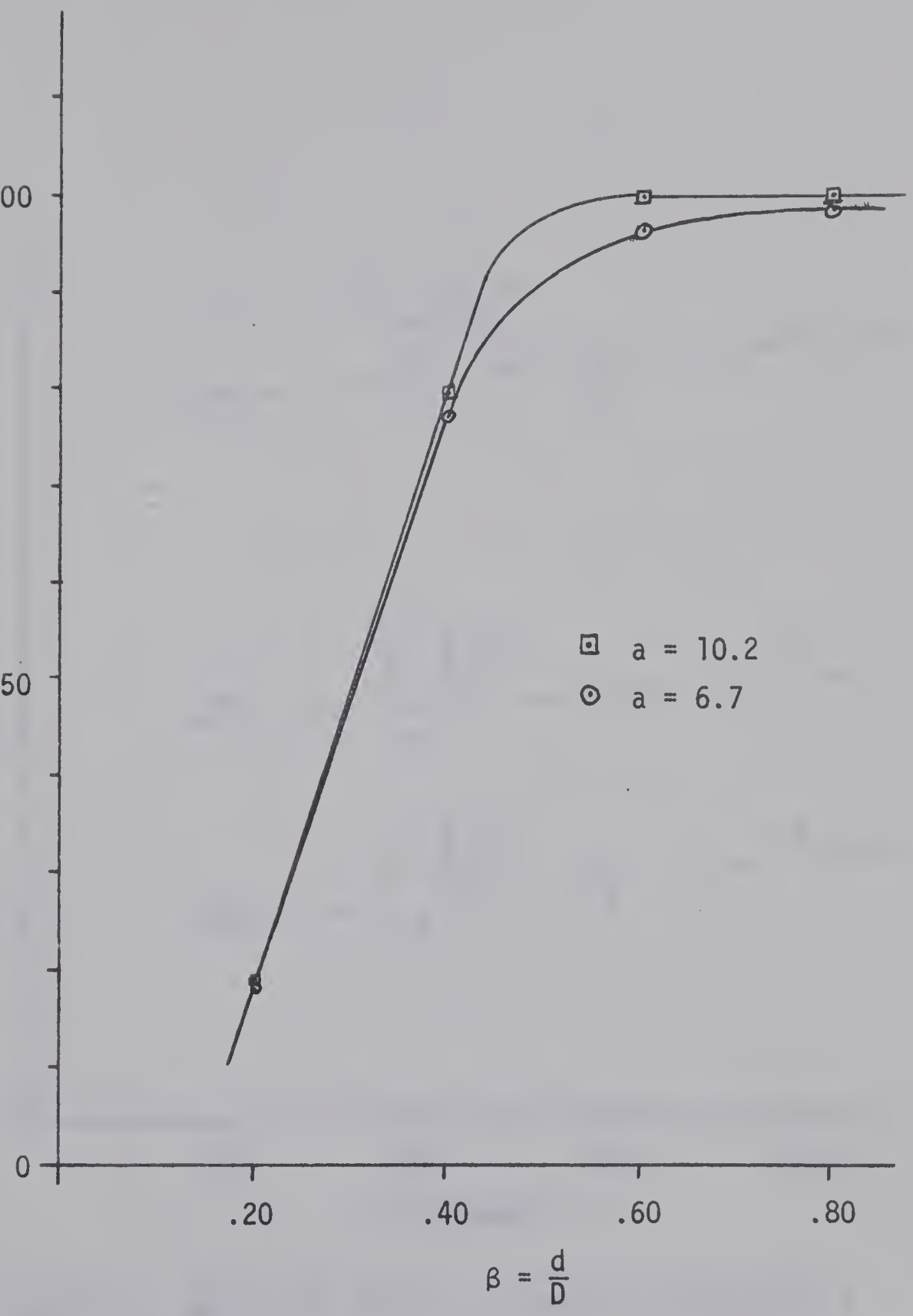

FIGURE 4.5 MASS FLOW RATIO γ vs DIAMETER RATIO β

AS A FUNCTION OF a $\theta = 50°$, $\lambda = 2.0$, Re = 1630

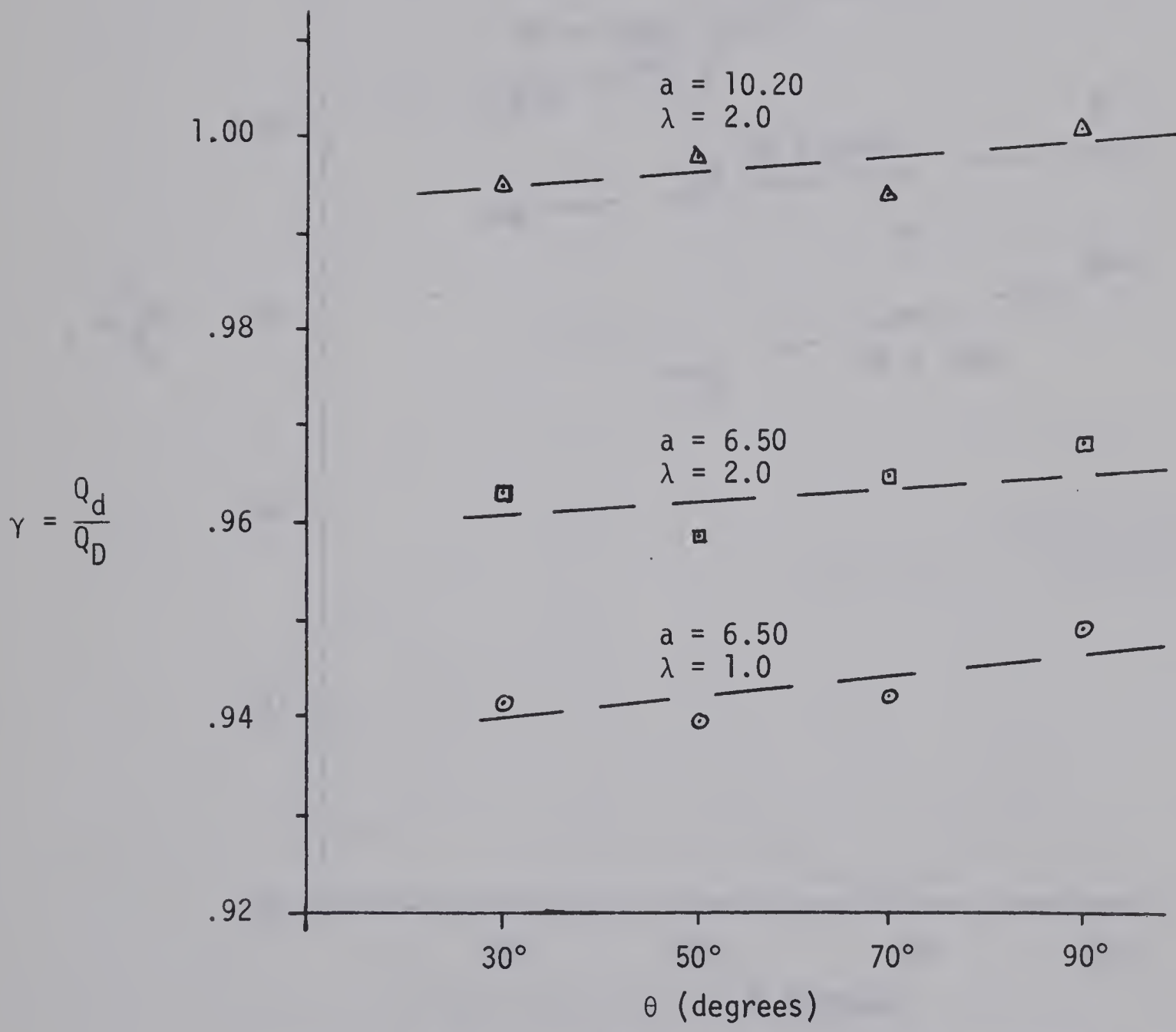

FIGURE 4.6 MASS FLOW RATIO γ vs ANGLE OF BRANCHING θ AS A FUNCTION OF a AND λ Re = 1630, β = 0.60

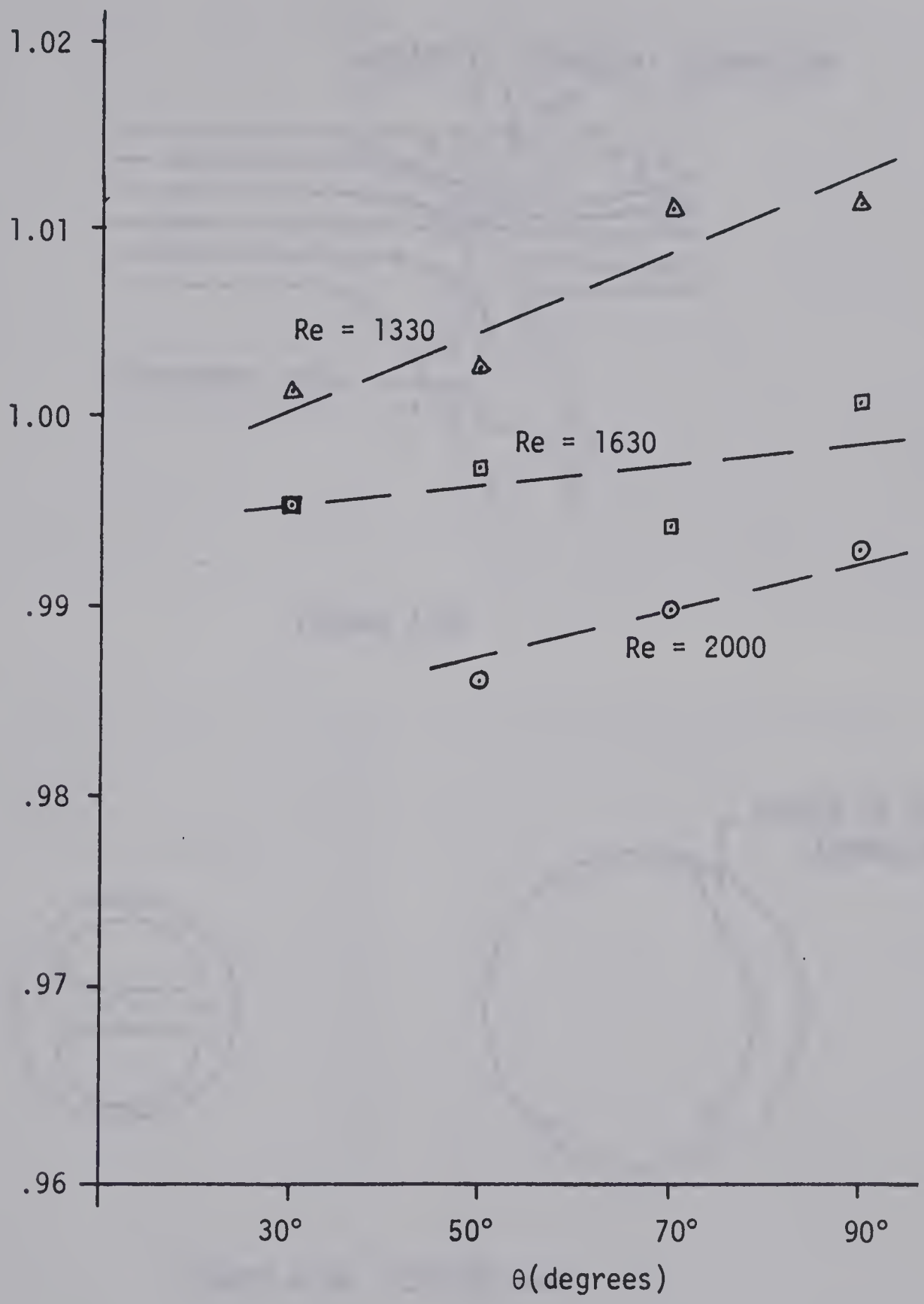

FIGURE 4.7 MASS FLOW RATIO γ vs ANGLE OF BRANCHING θ

AS A FUNCTION OF Re $a = 10.2$, $\lambda = 2.0$, $\beta = 0.60$

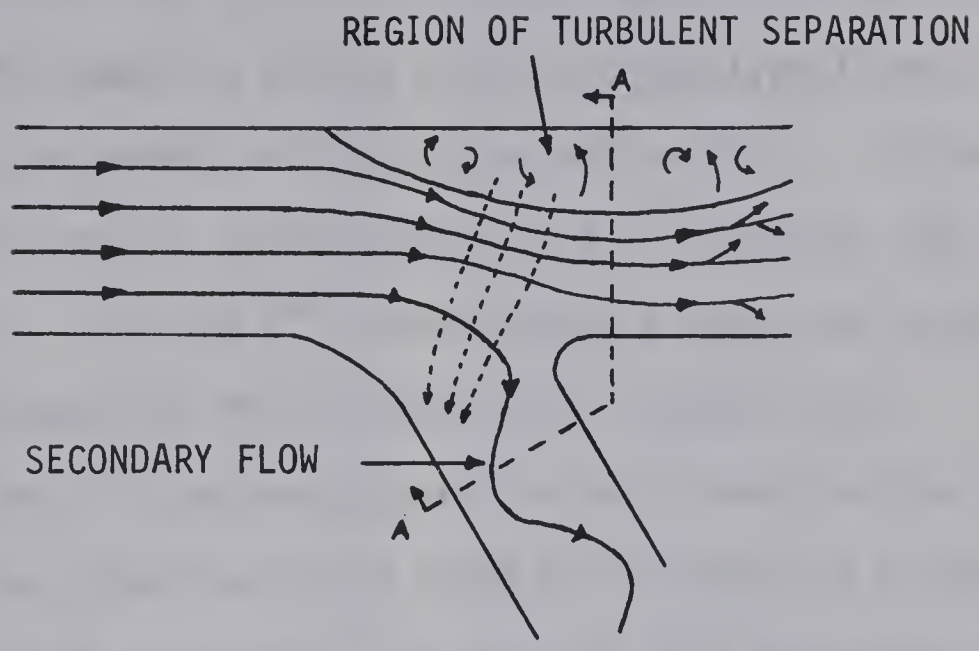

FIGURE 4.8a

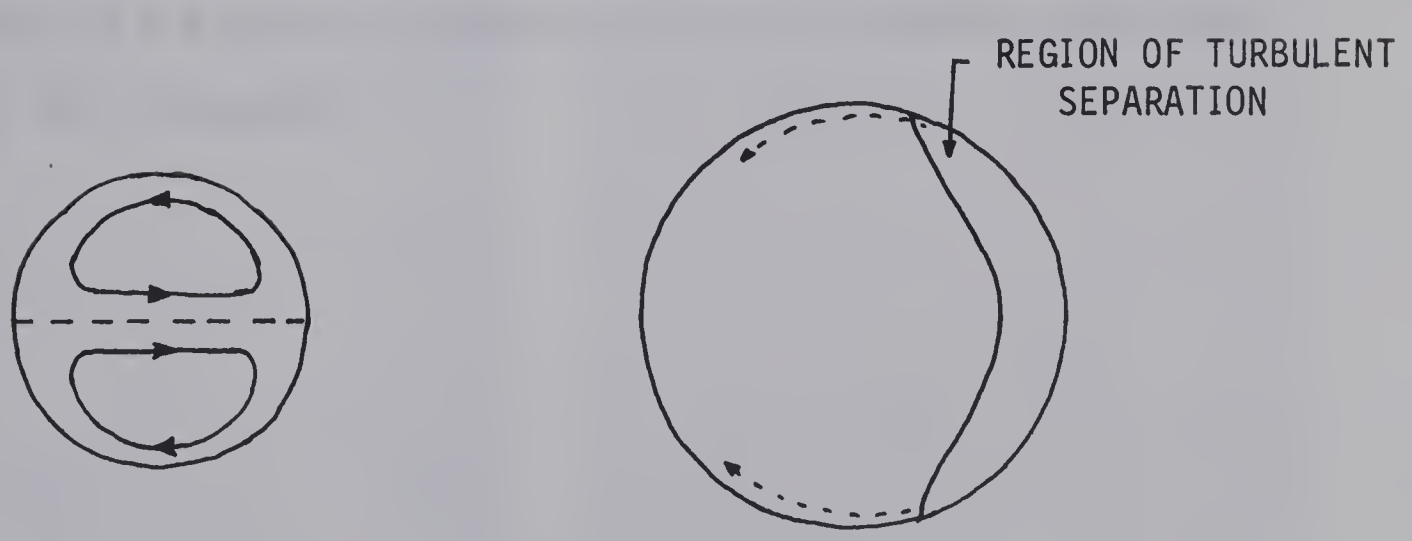

FIGURE 4.8b SECTION A-A

FIGURE 4.8 PHYSICAL DESCRIPTION OF THE FLOW

flow is set up from right to left along the top and bottom of the vessel wall. The composite effect is two helical-type flows, one in the top half of the vessel and one in the bottom half. This secondary flow was observed only in side branches of 0.75" diameter and smaller (see Figure 4.10). For the 1" diameter case, a region of turbulent separation was present at this location (see Figures 4.9).

A region of turbulent separation was present in the region of the main vessel opposite to the point of intersection of the side branch. Figure 4.8b illustrates the shape of this separated region. There was a small flow from this separated region to the side branch which is easily seen in Figure 4.10b.

Figures 4.9 and 4.10 illustrate the effect of Reynolds number (Re) and the angle of branching (θ) on the physical appearance of flow in the bifurcation.

FIGURE 4.9a $\theta = 90°$

FIGURE 4.9b $\theta = 70°$

FIGURE 4.9c $\theta = 50°$

FIGURE 4.9d $\theta = 30°$

FIGURE 4.9 FLOW CHARACTERISTICS FOR VARIOUS ANGLES OF BRANCHING
$\beta = 0.80$ Re = 1850

FIGURE 4.10a Re = 1920

FIGURE 4.10b Re = 1700

FIGURE 4.10c Re = 1570

FIGURE 4.10d Re = 1300

FIGURE 4.10 FLOW CHARACTERISTICS FOR VARIOUS REYNOLDS NUMBERS
$\beta = 0.60 \quad \theta = 50°$

CHAPTER V

CONCLUDING REMARKS

5.1 Observations and Discussion

Figure 4.1 indicates that the mass flow ratio (γ) is directly proportional to both the unsteadiness parameter (a) and the normalized component of the velocity fluctuation (λ). That is, γ increases as a increases and γ increases as λ increases.

A possible explanation for the dependence of γ on a stems from a statement by McDonald [3] (page 43) which reads as follows:

> "As the frequency increases, there is, as it were, less time in the cycle for the movement to be translated throughout the axial laminae and the velocity profile becomes very flattened".

Since a is directly proportional to the frequency, increasing a will flatten the velocity profile. Consequently, as a increases, proportionally more fluid will flow in the area near the outer walls than in the center of the vessel. Since flow in the side branch originates in the area proximal to the main vessel wall, a greater percentage of flow to the side branch results.

Turbulent flow has a much flatter velocity profile than has laminar flow (McDonald [3] page 23). Mitchell and Schwartz [5] and McDonald [3] recognize the existence of turbulent flow in a portion of the flow cycle and observations by the author of the experimental model corroborate this viewpoint. As λ increases, the magnitude of the maxi-

mum instantaneous velocity increases and it follows that the flow is turbulent for a greater portion of the cycle. This would result in a flattened velocity profile for a longer period of time and may be the reason for the increase in γ with increased λ.

Figure 4.2 indicates that, above a certain threshold a, γ is inversely proportional to the Reynolds number (Re). As the Reynolds number increases, the momentum of the fluid in the upstream branch increases, making it more difficult for the fluid stream to turn the corner into the side branch. Consequently, γ decreases. The author has been unable to develop a possible reason for the "threshold a" phenomenon.

As would be expected, Figures 4.3, 4.4, and 4.5 indicate that as the ratio of the diameters (β = d/D) increases, γ increases. Figures 4.1 and 4.2 indicate that an unfortunate choice was made for the constant values of a. If larger values of a had been chosen, the curves would not have been so close together and the relationships could have been viewed with greater clarity.

Figures 4.6 and 4.7 indicate a tendency for γ to increase as the angle of branching (θ) increases. Figure 4.9 illustrates a possible explanation for this phenomenon. As θ increases, the size of the separated region in the main branch appears to increase. This would tend to restrict flow in the main branch and could be the reason for the increase in γ.

Figures 4.9 and 4.10 indicate that changes in the physical appearance of the flow patterns are occurring as the Reynolds number and angle of branching are varied. However, it is difficult to say how these changes are related. The change most evident is the transition from a helical type flow in the 0.75" side branch (Figures 4.10) to a region of turbulent separation in the 1" side branch (Figures 4.9).

5.2 Summary

A generalized summary of the experimental findings of this thesis is as follows:

1. The mass flow ratio (γ) is directly proportional to the unsteadiness parameter (a) and the normalized velocity fluctuation (λ).

2. Below a threshold unsteadiness parameter (a = 8.5), the mass flow ratio (γ) is independent of the Reynolds number (Re). Above this threshold value, the mass flow ratio is inversely proportional to the Reynolds number.

3. The mass flow ratio (γ) is directly proportional to the ratio of the branch diameters ($\beta = d/D$).

4. The mass flow ratio appears to be directly proportional to the angle of branching (θ).

5.3 Suggestions for Further Work

During the course of any project, more efficient and improved methods of doing certain parts of the project are invariably found. This

is particularly true when one is attempting something that has never been done. Such was the case with this project which is unique, at least in this part of the country. Several changes from the original design of the apparatus were made, but the author found that time and money considerations made it impossible to make all the desired improvements. For this reason, several of the suggestions of this section are suggestions for improvements to the apparatus.

No extensive efforts were made to reproduce the experimental data. Before the experimental results are completely accepted, the author feels that several bifurcations of one particular geometry should be tested. In this way, any error caused by small discrepancies in the manufacture of the bifurcations should be negated.

One of the frustrating things about the experimental apparatus was the insensitivity of the flow adjustment. Successive readings for the total flow rate taken without adjusting the flow control valves would sometimes vary as much $\pm$ 2%. A more sensitive flow adjustment apparatus would contribute greatly to the accuracy of the experimental data and the mental state of the researcher.

By the end of the experiments, the once crystal-clear experimental fluid had become almost opaque. The author is not certain whether this was caused by breakdown of the resin particles or by exposure of the fluid to the environment in the open gathering tanks. For future work, it would be advisable to construct a covering for these tanks and to make the necessary flow observations soon after adding the resin

particles.

It has already been noted that there was a transition from a helical-type flow in the 0.75" side branch to a region of separation in the 1" side branch. Further information about this transition, such as the critical Reynolds number, could be obtained with new, more transparent fluid.

Although it was possible with the glass bifurcations to see the general flow characteristics, there was a considerable amount of distortion. A logical improvement would be the development of a distortion-free bifurcation. Photographs taken using such a bifurcation could be used to determine inlet and outlet velocity profiles using a method similar to Weiting's [16]. Kuchar and Ostrach [1] mention the need for information about velocity profiles.

Another possibility for future work would be pressure measurements. Not only would pressure plots taken upstream and downstream of the bifurcation be useful in themselves, but McDonald [3] has developed a technique for computing oscillatory flow rates from their pressure gradients. The gathering technique is very tedious and a faster more efficient flow measurement technique would be extremely useful.

The perfectly straight main branch of the experimental bifurcation does not occur physiologically. For this reason, the properties attributed to the experimental model may not hold for the physiological case. For example, curvature of the main branch may eliminate the region of separation found in that branch of the experimental model.

This idea could be investigated by examining models with main branches of various radii of curvature.

The side branch type junction considered in this thesis is only one example of the various geometries occurring physiologically. The Y-type branch could be examined by a similar experimental procedure.

As mentioned previously, a flexible junction would approximate the physiological case much better than the glass junction that has been used. A flexible junction must be developed before the arterial bifurcation can be completely simulated.

The work that has been suggested in this section is beginning this summer in the Department of Mechanical Engineering. With the exception of the flexible bifurcation, an attempt is being made to include all the suggested improvements. At this time, insufficient data is available to enable the author to speculate on the results of this work.

A characteristic of pulsatile flow is that its properties are highly dependent on pulse reflections. Pulse reflections are dependent on the geometry of the flow apparatus. Consequently, if the geometry of the experimental model was changed (eg. removal of the orifice plates), changes in the experimental results could be expected.

REFERENCES

1. N.R. Kuchar and S. Ostrach, "Flows in the Entrance Regions of Circular Elastic Tubes", Case Western Reserve University Publication No. FTAS/TR-65-3, Cleveland, 1965.
2. N.R. Kuchar and S.M. Scala, "Design of Devices for Optimum Blood Flow", ASME Publication No. 68-DE-52, 1968.
3. D.A. McDonald, "Blood Flow in Arteries", Edward Arnold (Publishers) Ltd., London, 1960.
4. R.L. Whitmore, "Rheology of the Circulation", Permagon Press Ltd., London, 1968.
5. J.R.A. Mitchell and C.J. Schwartz, "Arterial Disease", Blackwell Scientific Publications, Oxford, 1965.
6. H.B. Atabek, "End Effects", from "Pulsatile Blood Flow" by E.O. Attinger (editor), McGraw-Hill Book Co., 1964.
7. R.L. Evans, K.F. Hosie, R.H. Kooiker, J. Perry, and R.J. Stish, "Reflections in model and arterial pulse waves", Journal of Applied Physiology 15(2):258-260, 1960.
8. G.S. Malindzak Jr., "Reflection of Pressure Pulses in the Aorta", Medical Research Engineering Vol. 6, Fourth Quarter, 1967.
9. R.H. Cox, "Comparison of Linearized Wave Propagation Models for Arterial Blood Flow Analysis", ASME Publication No. 69-BHF-15, 1969.

10. L.J. Krovetz, "The Effect of Vessel Branching on Haemodynamic Stability", Phys. Med. Biol. Vol. 10, No. 3, pp. 417-427, 1965.

11. D.J. Scheck and W.H. Gutstein, "Boundary Layer Studies in Blood Flow", ASME Publication No. 66-WA/BHF-4, 1966.

12. H. Schlichting, "Boundary Layer Theory", McGraw-Hill Book Co., 1968, Sixth Edition.

13. M.M. Wintrobe, "Clinical Haematology", Lea and Febiger, Philadelphia, 1968.

14. W.W. Tuttle and B.A. Schottelius, "Textbook of Physiology", The C.V. Mosby Company, St. Louis, 1965.

15. Bell, Davidson, and Scarborough, "Textbook of Physiology and Biochemistry", E.&S. Livingstone Ltd., Edinburgh and London, 1965, Sixth Edition.

16. D.W. Weiting, "A Method of Analyzing the Dynamic Flow Characteristics of Prosthetic Heart Valves", ASME Publication No. 68-WA/BHF-3, 1968.

17. E. Hatschek, "The Viscosity of Liquids", G. Bell & Sons, London, 1928.

APPENDIX A

SPECIFIC GRAVITY AND VISCOSITY OF THE BLOOD ANALOGUE

The blood analogue used was a mixture of glycerine and water which was 36.7% glycerine by volume. The specific gravity of glycerine, measured with an Exax Heavy Liquid Hydrometer, was 1.270.

Therefore, specific gravity of the mixture

= .367 (1.270) + .633 (1.000)

= .466 + .633

= 1.10

The weight percent of glycerine of the mixture

$$= \frac{.466}{1.10} = .424$$

Hatschek [17] compiled data for the viscosity of various mixtures of glycerine and water at several temperatures. Table A.1 is reprinted from his book. The viscosity of a 42.4% by weight glycerine-water solution at 20°C is required. Values for a 39.31% and 99.14% solution at 20°C were not tabulated. Values for these solutions were obtained by interpolation from Figures A-1 and A-2 which are plots of viscosity versus temperature for 39.31% and 99.14% solutions respectively. From Figure A-3, a plot of viscosity versus weight percent of glycerine, the viscosity of the blood analogue is 4.5 centepoise.

This viscosity was checked by a Brookfield "Synchro-Lectric"

TABLE A.1 VISCOSITIES (in centepoise) OF VARIOUS GLYCERIN WATER MIXTURES

	Weight Percent Glycerin					
Temp. °C	99.14	81.98	61.44	39.31	20.29	0
17	--	100.7	--	--	--	--
18	1393.0	--	--	3.89	2.03	--
20	1260**	72.6	12.27	3.7*	1.90	1.029
30	570.8	40.3	8.57	2.84	1.58	0.817
40	267.5	25.5	5.75	2.11	1.19	0.672
50	175.2	15.1	4.19	1.69	0.97	0.550
60	124.1	12.2	3.23	1.37	0.86	0.455
70	53.3	8.61	2.56	1.16	0.72	0.403
80	32.8	5.68	2.04	1.01	0.64	0.351
90	17.9	5.01	1.69	0.88	0.55	0.317

* - From Figure A.1

** - From Figure A.2

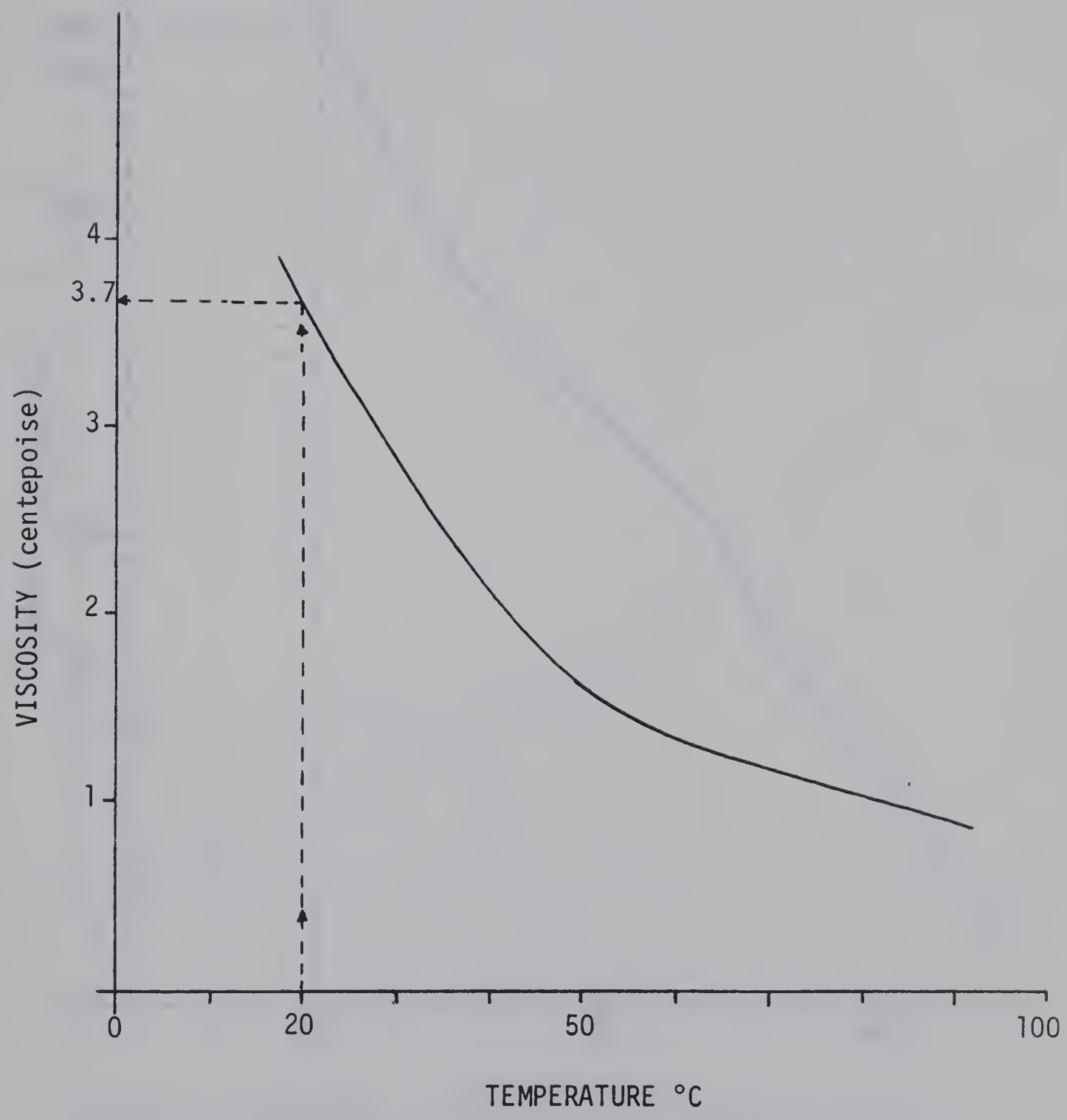

FIGURE A.1 VISCOSITY vs TEMPERATURE OF 39.31%
(by weight) GLYCERIN/WATER MIXTURE

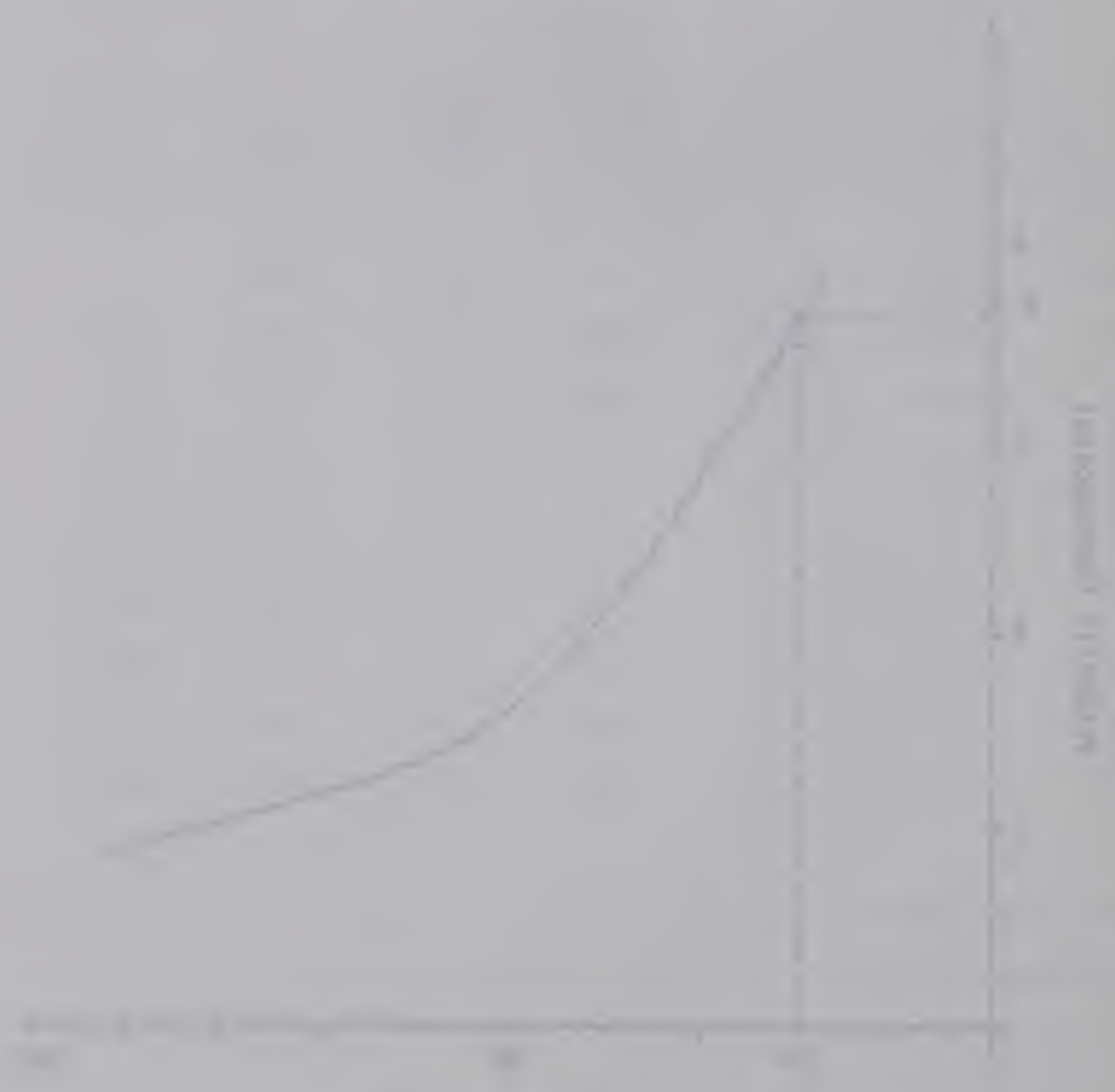

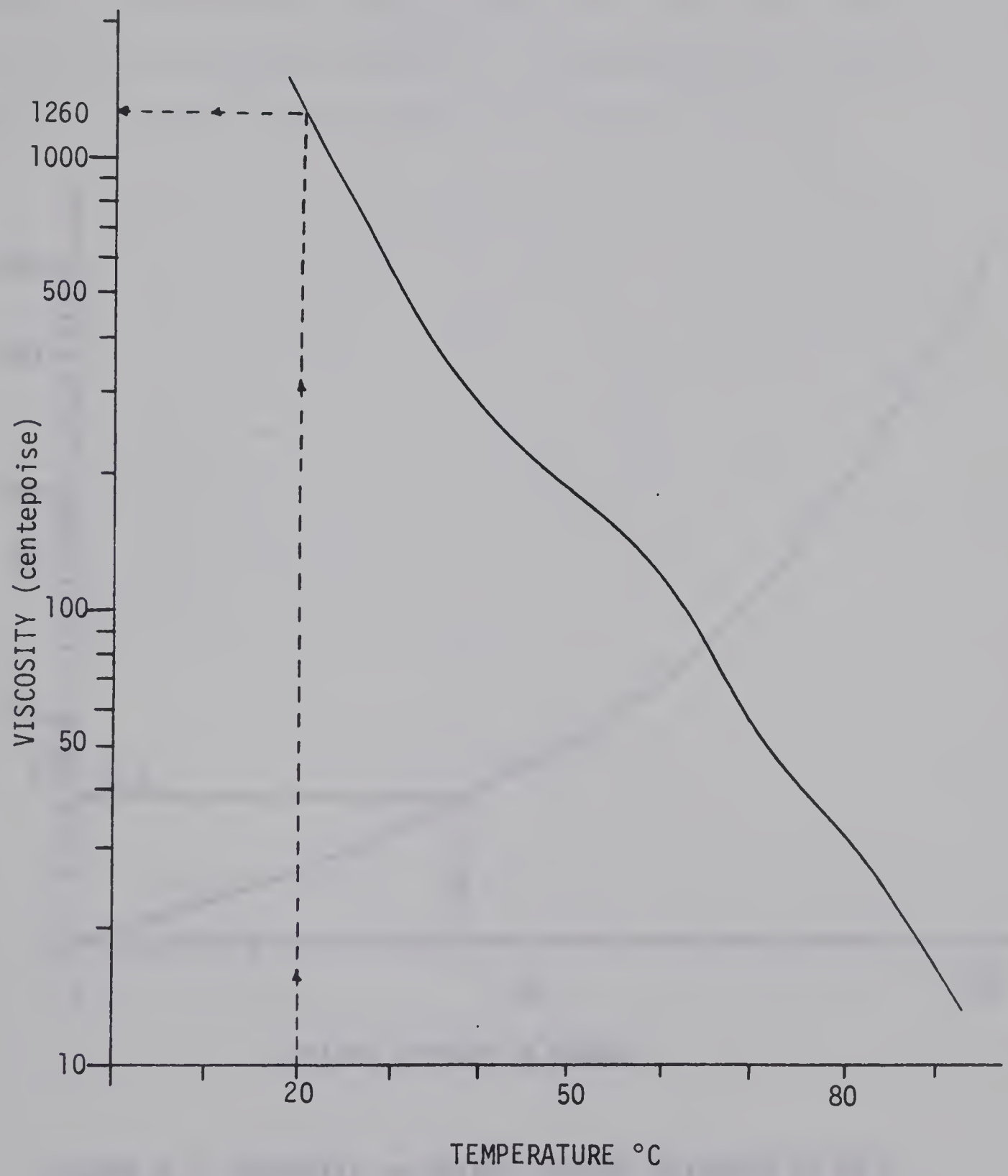

FIGURE A.2 VISCOSITY vs TEMPERATURE OF 99.14%

(by weight) GLYCERIN/WATER MIXTURE

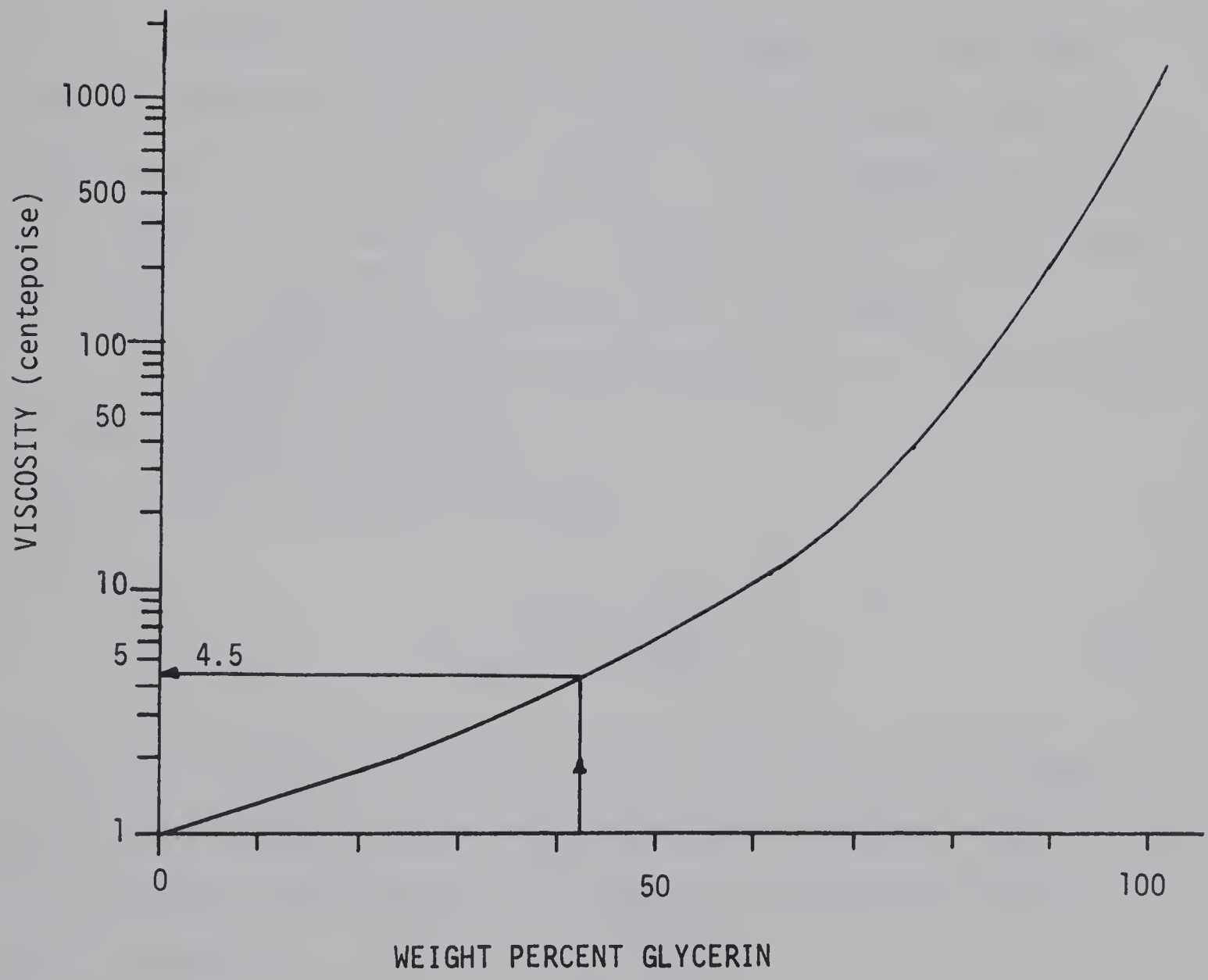

FIGURE A.3 VISCOSITY vs WEIGHT PERCENT GLYCERIN AT 20°C

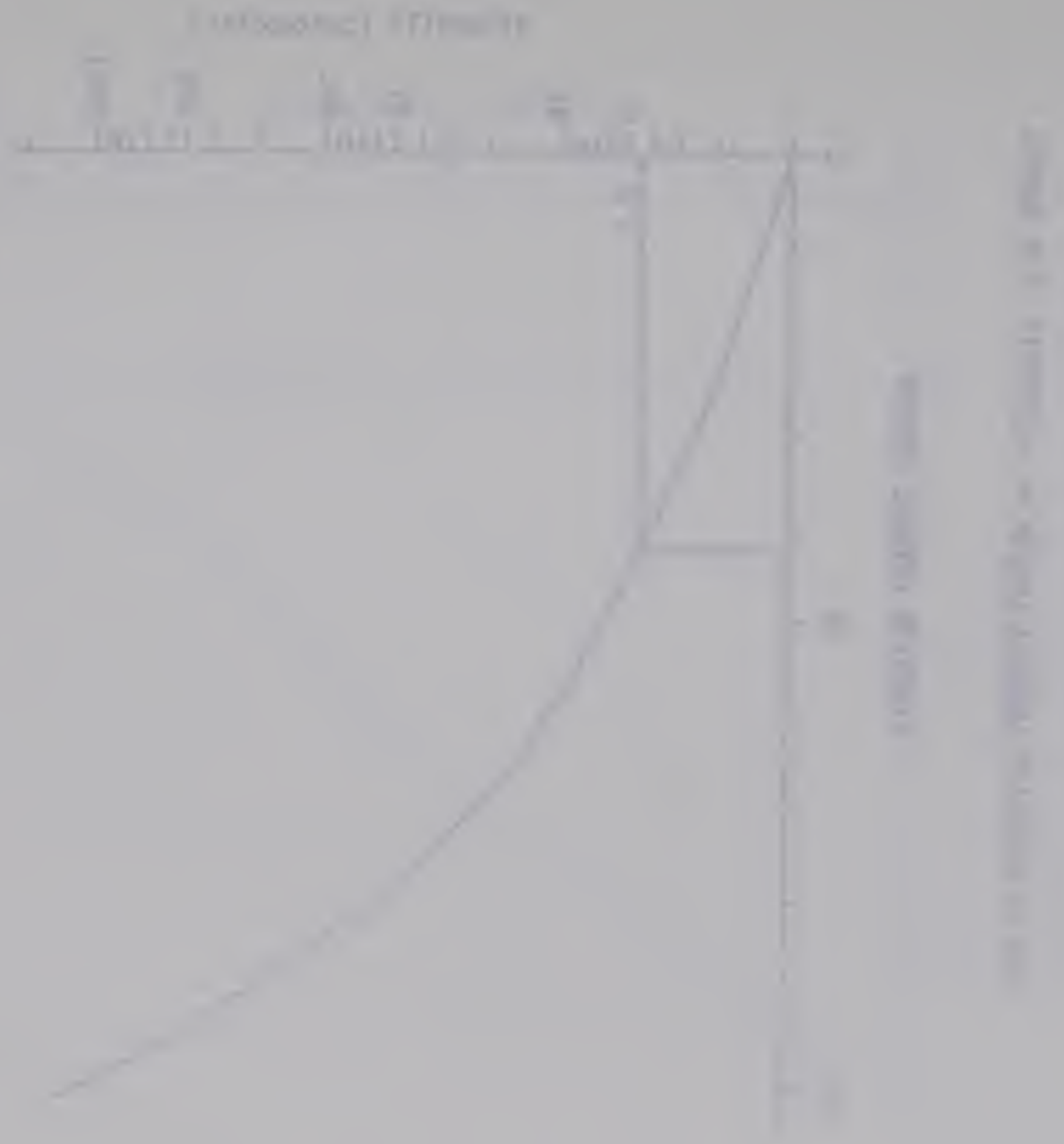

Viscometer and a Fann Model 35 Viscometer. The accuracy of these instruments in the required range was rather poor, but they served to corroborate the calculated viscosity. No appreciable difference in readings was evident with the addition of the resin particles.

APPENDIX B

PISTON STROKE CALCULATIONS

In order to study the effect of changes in the normalized velocity fluctuation, the length of the piston stroke was varied by using cams of different sizes. However, λ is also dependent on the pulse rate ω and the flow rate Q. That is, the value of λ will change if ω or Q is changed, even though the cam is not changed.

To determine the relationship between Q, ω, λ, and the length of stroke ℓ, consider Figure B-1.

The instantaneous flow rate

$$= Q + \frac{Q'}{2} \sin \left(\frac{2\pi}{T_o}\right) t \qquad (B.1)$$

where Q' is fluctuating component of the flow rate, T_o is the time required to complete one pulse, and t is the time variable. Since Q and Q' are directly proportional to the velocity U and fluctuating component of velocity U',

$$\lambda = \frac{U'}{U} = \frac{Q'}{Q}$$

Therefore,

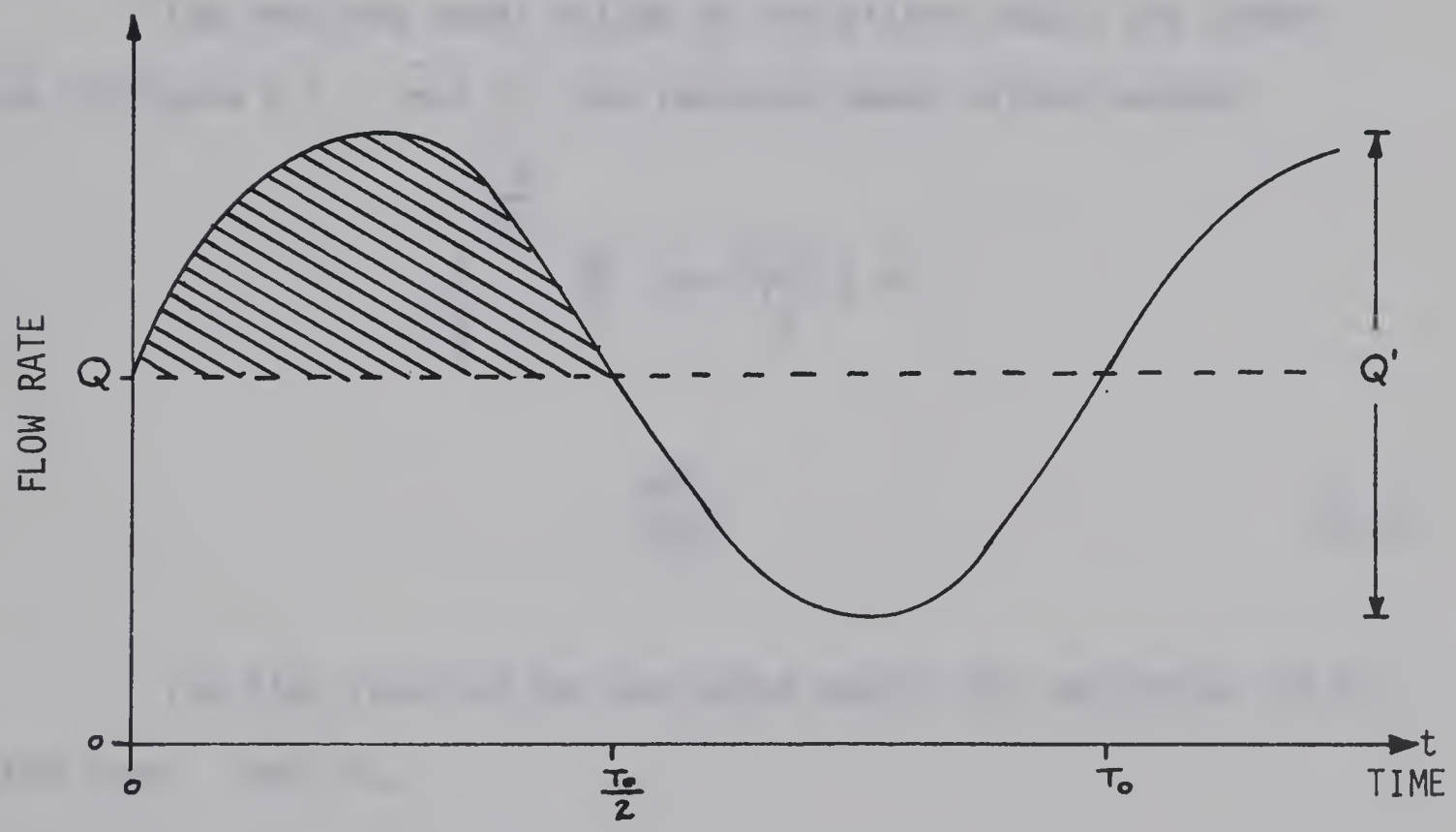

$$\lambda = \frac{Q'}{Q}$$

FIGURE B.1 FLOW IN THE EXPERIMENTAL MODEL

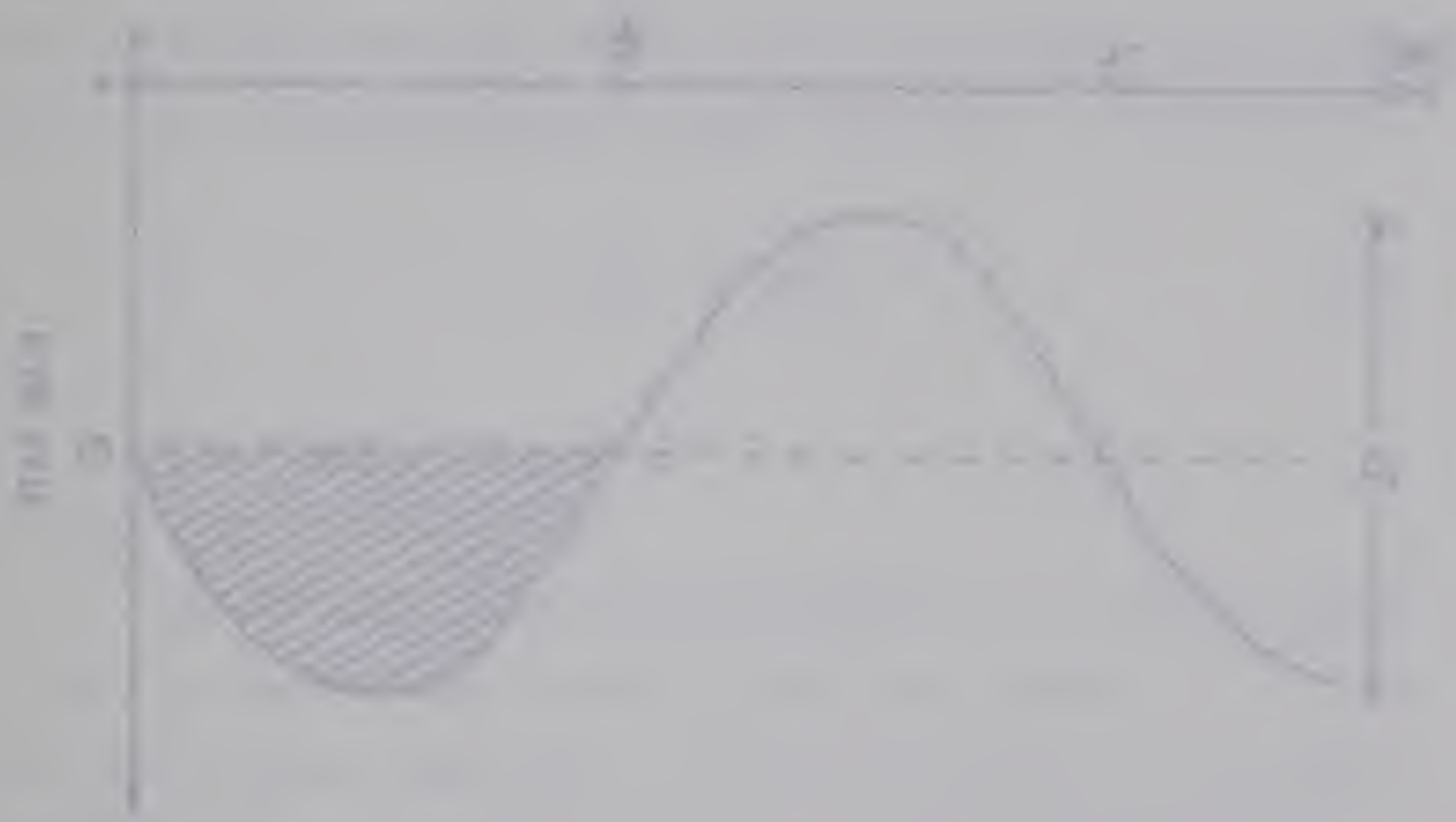

$$Q' = \lambda Q \tag{B.2}$$

Substituting (B.2) into (B.1) the instantaneous flow rate becomes

$$Q\left[1 + \frac{\lambda}{2} \sin\left(\frac{2\pi}{T_o}\right) t\right]$$

The required swept volume of the piston equals the shaded area of Figure B.1. That is, the required swept volume becomes

$$\int_0^{\frac{T_o}{2}} \frac{\lambda Q}{2} \sin\left(\frac{2\pi}{T_o}\right) t \, dt$$

$$= \frac{\lambda Q T_o}{2\pi} \tag{B.3}$$

The time required for one pulse equals the reciprocal of the pulse rate. That is,

$$T_o = \frac{1}{\omega} \tag{B.4}$$

Substituting (B.4) into (B.3), the required swept volume becomes

$$\frac{\lambda Q}{2\pi\omega} \text{ gal.}$$

The required length of stroke ℓ is obtained by dividing by the cross-sectional area of the piston (diameter = 4") and applying the appropriate conversion factors. That is,

$$\ell = \frac{\frac{\lambda Q}{2\pi\omega} \text{ gal.} \times .1605 \frac{\text{ft}^3}{\text{gal}} \times 1728 \frac{\text{in}^2}{\text{ft}^3}}{\pi(2)^2 \text{ in.}^2}$$

$$\ell = 3.5 \frac{\lambda Q}{\omega} \text{ in.}$$

APPENDIX C

CAM DESIGN

Numerous cams were used during the course of the experiments. They are described (by length of stroke) in Chapter IV. Figure C.1 illustrates how these cams were designed. To achieve the desired sinusoidal motion, a sine wave is plotted. The cam dimensions are obtained by measuring the difference between the base line and the sine curve. This dimension is then transferred to the diagram of the cam itself and measured off at the appropriate angle.

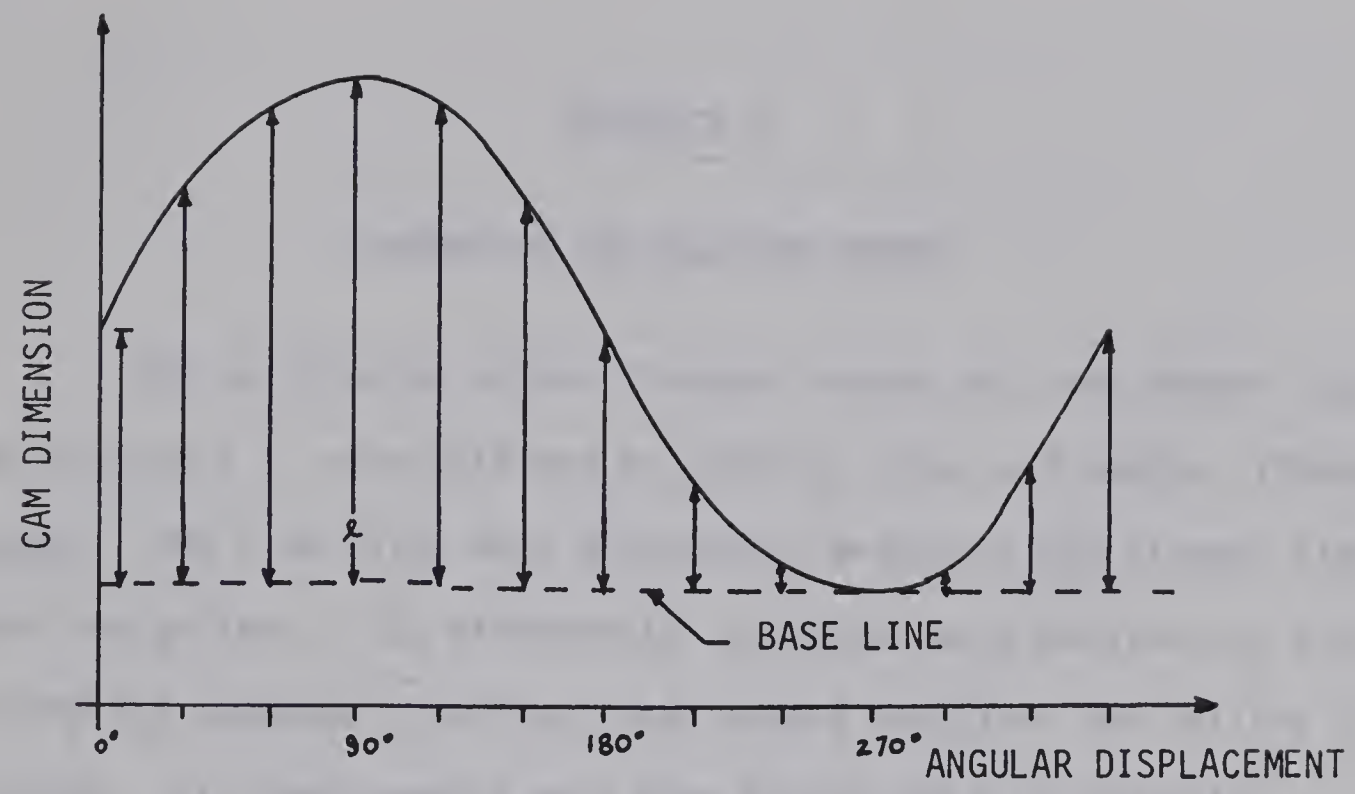

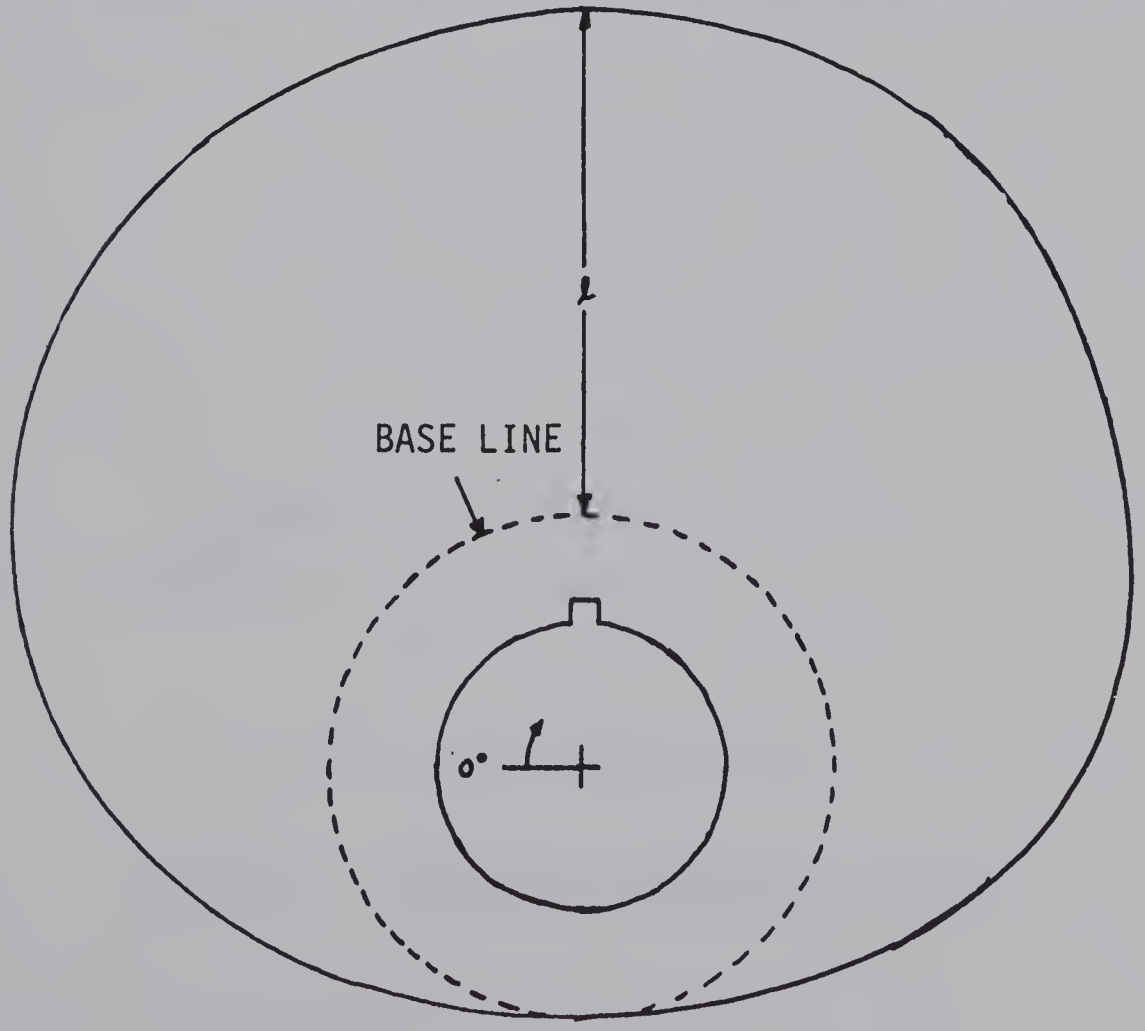

FIGURE C.1 CAM DESIGN

APPENDIX D

MANOMETER CALIBRATION CURVES

The calibration curves for main branch and side branch flow rates (Figure D.1) were obtained by plotting flow rate versus differential pressure. The flow rates were obtained by measuring the elapsed time to gather two gallons. The differential pressures were obtained by subtracting the manometer readings taken before and after the orifice in each line. All measurements were made during non-pulsatile flow.

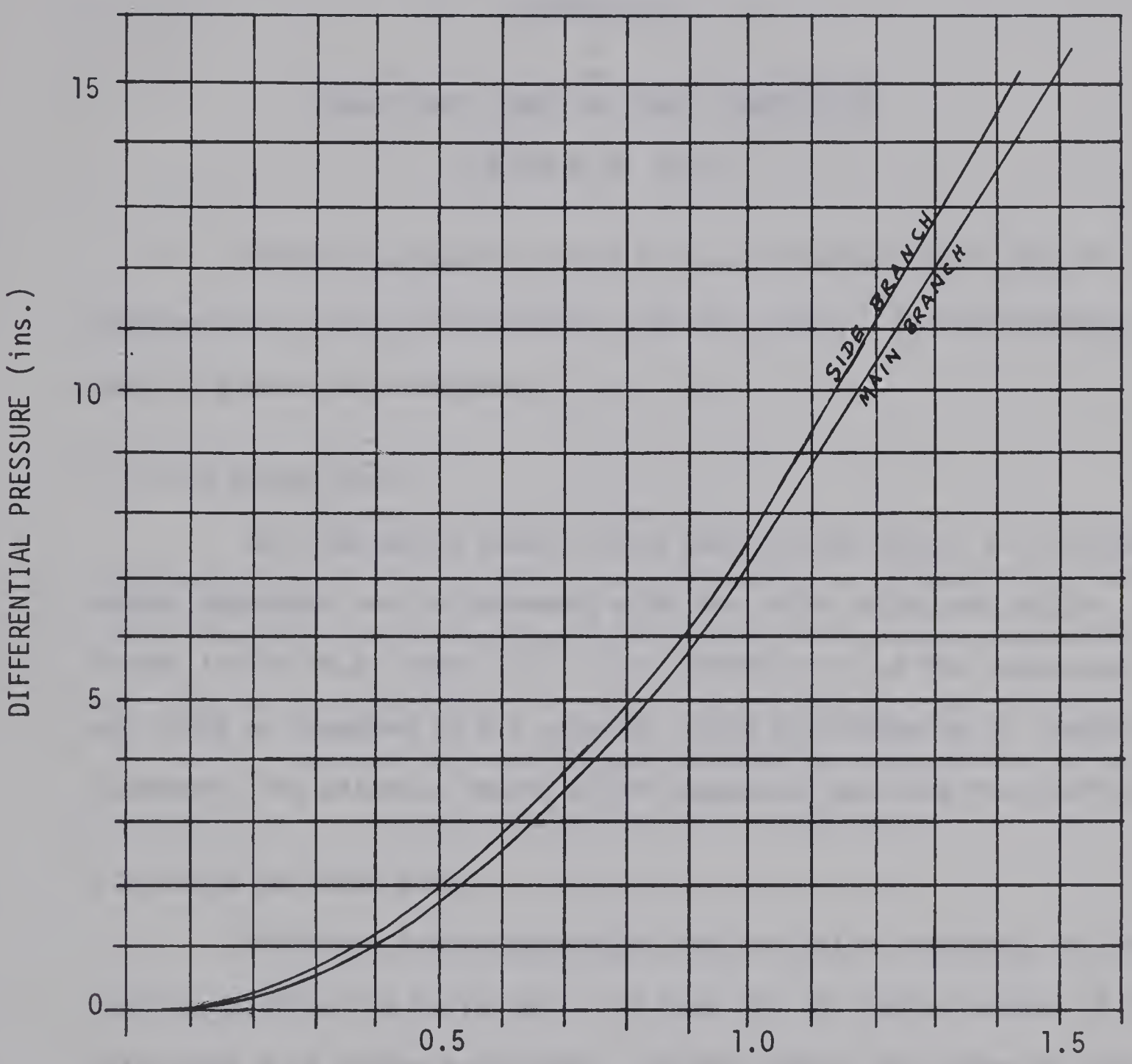

FIGURE D.1 MANOMETER CALIBRATION CURVES

APPENDIX E

SUGGESTIONS FROM THE ORAL EXAMINATION (DEFENSE OF THESIS)

Several suggestions from the oral examination of July 30, 1970 were not easily incorporable into the thesis. For convenience they have been included here.

E.1 The Length Ratio

Dr. Rodkiewicz asked if the length ratio (R_0/L) of the experimental apparatus was in agreement with the value calculated by Dr. Kuchar in his Ph.D. thesis [1]. The length ratio of the apparatus was .0065 as compared to the value of .0193 calculated by Dr. Kuchar. Therefore, the entrance length of the apparatus was more than sufficient.

E.2 Units of Pulse Rate

Professor Sadler expressed some confusion regarding the units used to describe the pulse rate. On page 25, the author speaks of the pulse rate ω in cycles per minute. At this point, the range of study for ω is being calculated and w refers specifically to the pulse rate of the human heart. From this point onwards, ω is measured in revolutions per minute (r.p.m.). This is because the author is now referring to the necessary angular velocity of the cam in the experimental model.

E.3 Dr. Laurenson's Suggestions

During the course of the examination, Dr. Laurenson of the Department of Anatomy made several suggestions which the author feels should be recorded here in the interest of future researchers.

Dr. Laurenson briefly discussed the possibilities of making flow observations by the use of cine film and split screen television. Cine film would enable a researcher to study the bifurcation flow phenomena in slow motion. With the help of split screen T.V., a suspended resin particle could possibly be viewed from the side and from above to give a better idea of its three-dimensional motion.

Dr. Laurenson suggested that heparinized low blood could possibly be used as an alternate experimental fluid. Some difficulties might be incurred, however, because of changes in the blood properties due to the heparin addition.

Dr. Laurenson also expressed the need for research into how the arterial wall is damaged by various flow phenomena.